Low-energy ion scattering : imaging characteristics of the EARISS apparatus and "Static LEIS"

Bergmans, R.H.

Award date:
1991

Low-Energy Ion Scattering: Imaging characteristics of the EARISS apparatus and "Static LEIS"

R.H. Bergmans **February 1991**

Master thesis
Eindhoven University of Technology
Department of Physics
Solid State Division
Surface and Interface Physics Group

Coached by prof. dr. H.H. Brongersma and dr. R.G. van Welzenis

Summary

Low-Energy Ion Scattering (LEIS) is a surface sensitive technique. In LEIS inert gas ions are directed onto a surface. From the energy distribution of the scattered ions the composition of the surface can be determined and from the azimuthal distribution surface structural information is obtained.

EARISS (Energy and Angle Resolved Ion Scattering Spectrometer) is a novel type of LEIS apparatus, which measures the energy and azimuthal distributions of the scattered ions simultaneously. This gives a two-dimensional image where every point, (E,ϕ), corresponds to a certain energy and azimuth.

The imaging characteristics of EARISS have been investigated by performing measurements on a Ni(100) sample. The energy axis of the obtained two dimensional image confirms to be linear. Further, the energy resolution was good enough to observe the Ni-isotopes when using 3 keV Ne^+ ions. The azimuthal distribution was expected to be homogeneous but a peaked structure was observed, probably caused by EARISS itself.

Because of the simultaneous measurement of the energy and azimuth of the scattered ions, it is possible to perform measurements with extremely low ion doses. From measurements performed at extremely low ion doses, it can be concluded that even non-destructive measurements on polymers (which are easily damaged) are possible with EARISS.

A measurement of 2 keV Ne^+ ions on $Au_{20}Pd_{80}$ (the peaks are separated by 382 eV) was done, to show that EARISS is capable of imaging several elements simultaneously.

Dankwoord

Gaarne wil ik iedereen bedanken die heeft bijgedragen tot het tot stand komen van dit afstudeerverslag. In het bijzonder wil ik een aantal personen noemen.

Allereerst mijn afstudeer hoogleraar Hidde Brongersma en Rob van Welzenis voor hun begeleiding, ondersteuning en de zeer plezierige samenwerking tijdens mijn afstuderen. Ook de hulp en snelheid van de groep technicus Gerard Wijers was onontbeerlijk tijdens mijn afstuderen. Verder wil ik Piet van den Hoogen en Jos de Laat bedanken voor hun vakmanschap bij het uitvoeren van reparaties en wijzigingen aan de opstelling. De leden en genoten van het dispuut Charm wil ik bedanken voor de getoonde belangstelling. Tenslotte wil ik nog mijn ouders bedanken voor hun interesse en steun tijdens mijn studie.

Rob Bergmans

List of contents

Chapter 1

Introduction

Surfaces play a crucial role in chemical reactions, catalysis, adhesion, crystal growth, wear, bonding and numerous other technologically and scientifically interesting processes. A better understanding of the surface is, therefore, of great importance to modern technology.

The development of ultra high vacuum (UHV) technology in the late sixties, was a great step forward in surface science. UHV conditions made it possible to prepare clean surfaces and to keep the contamination of the surfaces below an acceptable level during the measurements.

Since then, the increase in surface analytical techniques has been enormous. In these techniques a primary beam of particles or sonic surface waves are incident on the surface or a thermal, electrical or magnetic field is applied to the surface. The particles that are scattered or emitted by the surface are the subject of investigation. To illustrate this, we show the fundamental basis of surface analytical techniques in fig. 1.1.

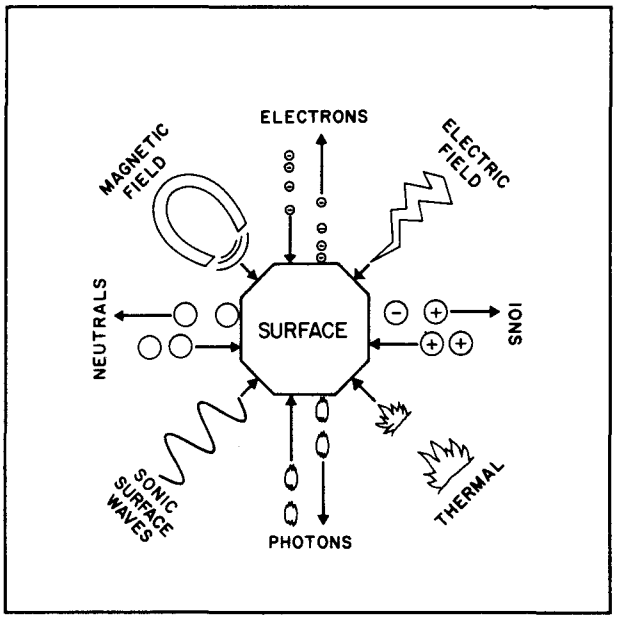

Figure 1.1: Pictorial representation of surface analysis techniques [CZA75].

In analyzing the emitted particles, one can consider five possible types of information; identification of the particle, state of the particle, spatial distribution, energy distribution and number. For a good understanding of the surface one has to combine several techniques, since they all have there characteristic advantages and drawbacks. For a discussion of the variety of surface analytical techniques we refer to textbooks (for example [CZA75] and [WAL89]).

The technique that is used in this thesis is Low Energy Ion Scattering (LEIS). In LEIS a primary beam of inert gas ions with low energies (0.1 - 10 keV) is incident on the surface, see fig. 1.2.

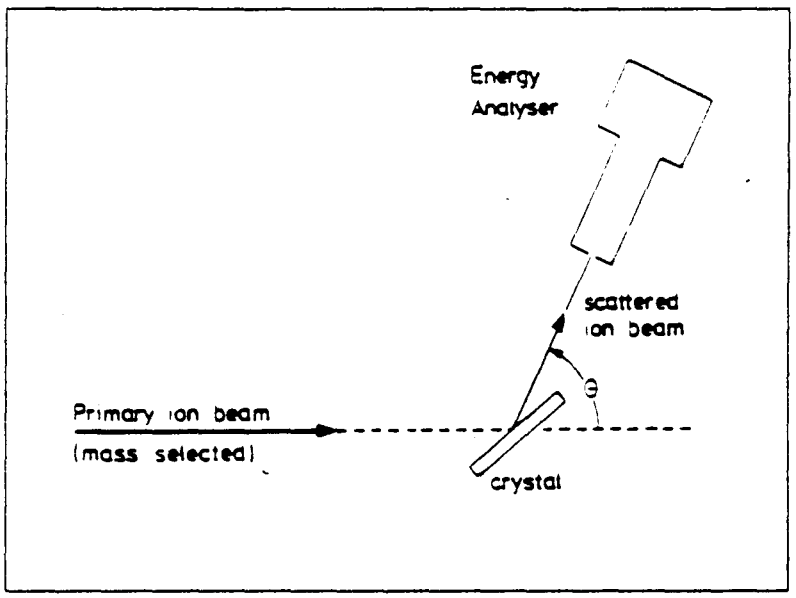

Figure 1.2: Simple LEIS experiment, showing an ion beam directed to a sample and an analyzer and detector to measure the energy of ions scattered over an angle θ.

The energy losses of ions that scatter of the surface depends on the masses of the surface atoms. Therefore, information about the elemental composition of the surface can be obtained from the energy distribution of the scattered ions. By considering the direction of scattered ions, it is possible to determine the surface atomic structure. The information obtained with LEIS is limited to one or two atomic layers which makes it extremely surface sensitive. The reason for this is the high neutralisation probability of inert gas ions.

One of drawbacks of LEIS is the damage to the surface due to incident ions. This means that the ion dose has to be kept to a minimum. For this reason the EARISS (Energy and Angular Resolved Ion Scattering Spectroscopy) apparatus, which makes a much more efficient use of the scattered ions than a conventional LEIS apparatus, is being developed.

The contents of this thesis can be summarized as follows. It starts with an explanation of the physical principles of LEIS in Chapter 2. Then it continues with a description of the EARISS apparatus in chapter 3. The measurements shown in chapter 4 were performed to investigate some of the energy and azimuthal imaging capabilities of EARISS and in chapter 5 measurements are shown with extremely low ion doses. Chapter 6 deals with a problem of the EARISS detector and some conclusions and recommendations are given in chapter 7.

Chapter 2

Physical Background

2.1 Introduction

Low-energy ion scattering (LEIS) is a surface sensitive technique with the ability to obtain information about the composition and atomic arrangements of surfaces. In LEIS ions with a fixed energy are directed onto a surface. From the energy distribution and the yield of the scattered ions the above mentioned information can be deduced. The basis for this is that in LEIS it is easy to relate the mass of a surface atom to the energy of the scattered ion. Further because the atoms can be thought of as biljart balls structural information can be obtained by considering shadowing and blocking effects amongst the surface atoms, or multiple collisions of the incident ion. When using noble gas ions the obtained information will be limited to the outermost atomic layer due to the high neutralisation probabilities of these ions. Furthermore, the sensitivity of LEIS for the different elements differ because of different cross sections and neutralisation processes.

2.2 The binary collision model

The relationship between the energy of the scattered ions and the masses of the surface atoms can be obtained using a simple binary collision model based on classical mechanics, see fig. 2.1.

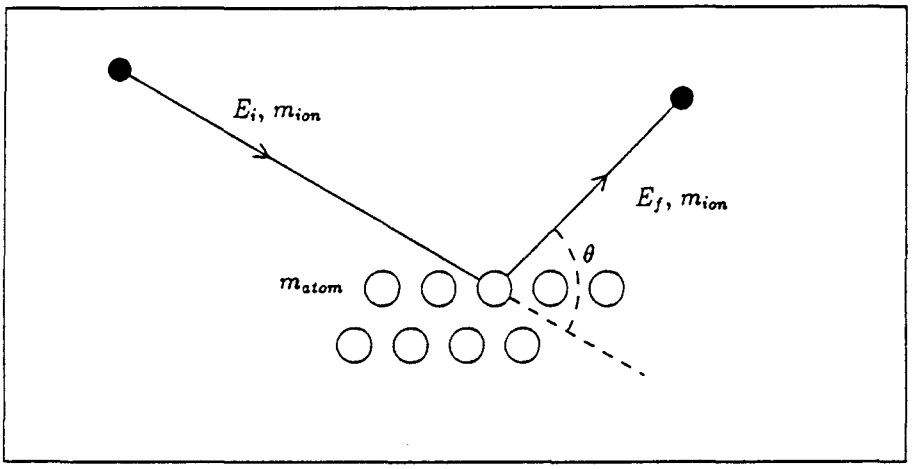

Figure 2.1: Schematic representation of the collision of an ion with an atom in the surface [ACK90].

The reason that this model works quite well can be elucidated as follows.

- The de Broglie wavelength of the keV ions is very small compared to the interatomic distances between the surface atoms, therefore, diffraction effects can be neglected.
- The distance of closest approach is very small compared to the interatomic distances and, therefore, the collisions can be assumed to be binary.
- The collisions between the ions and the target atoms can be described by an interatomic repulsive potential between them; a screened coulomb potential is used. This means that the collision can be assumed to be elastic.
- The target atom can be assumed to be at rest because the vibration time (10^{-13}s) is much larger than the interaction time (10^{-15}s - 10^{-16}s).

Application of the energy and momentum conservation laws for a single binary collision gives the following expression for the energy retained by the scattered ion:

$$E_f = E_i \left[\frac{\cos\theta \pm \sqrt{q^2 - \sin^2\theta}}{1+q} \right]^2 \qquad (2.1)$$

Here q is the ratio of the target and projectile masses ($q = M_{atom}/M_{ion}$), see fig. 2.1. This equation only gives a physical solution for $q^2 \geq \sin^2\theta$. For $q > 1$ only the positive sign applies and for $q \leq 1$ both signs give a physical solution.

Equation (2.1) can be represented by using a polar diagram as shown in fig. 2.2.

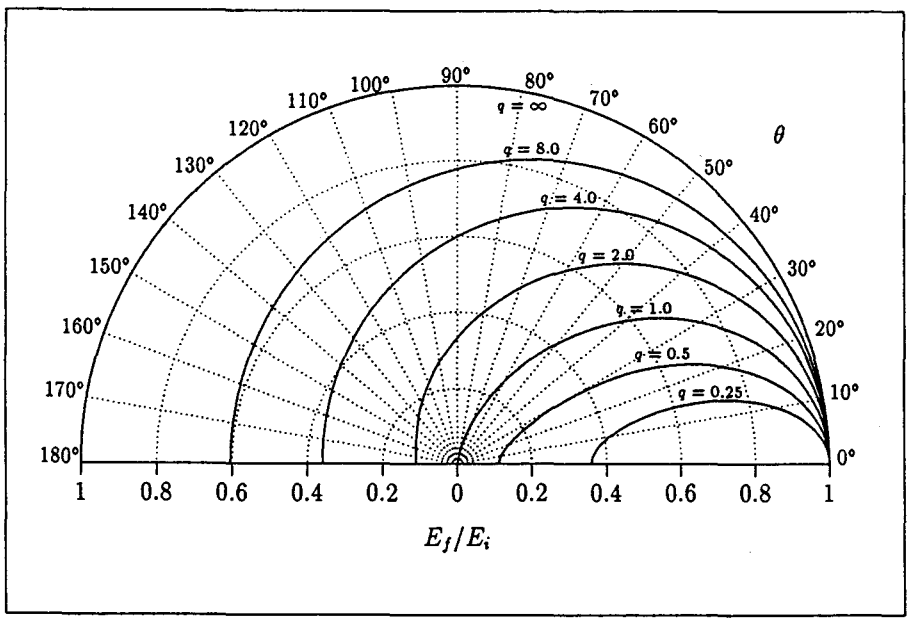

Figure 2.2: Polar diagram of the ratio of final and incident energy at various scattering angles and q-values [ACK90].

In this polar diagram the ratio E_f/E_i is displayed as a function of the scattering angle for several q values. As can be seen from this diagram the mass resolution increases for large scattering angles and small values of q. This means that for high mass resolution LEIS configurations with large scattering angles have to be

used, but one has to keep in mind that only elements which are heavier than the incident ions (q > 1) can be seen for scattering larger than 90°. Furthermore, the mass resolution can be improved by choosing heavier incident ions although this decreases the number of elements that can be seen (q >1) and it increases the surface damage. For values of q close to one E_f is very small and this means an extremely high neutralisation probability, see equation 2.5 further on. Therefore, in practice only elements for which q > 2.5 will be observed.

The two possible solutions for q < 1 can be seen directly in the polar diagram. The solution for the smaller E_f/E_i value is the result of a nearly head-on collision and the other one of a grazing collision.

The energy spectrum

Besides the ions that scatter off the surface two other type of ions can be detected. In fig. 2.3 this is illustrated by a LEIS spectrum of a surface with only one element.

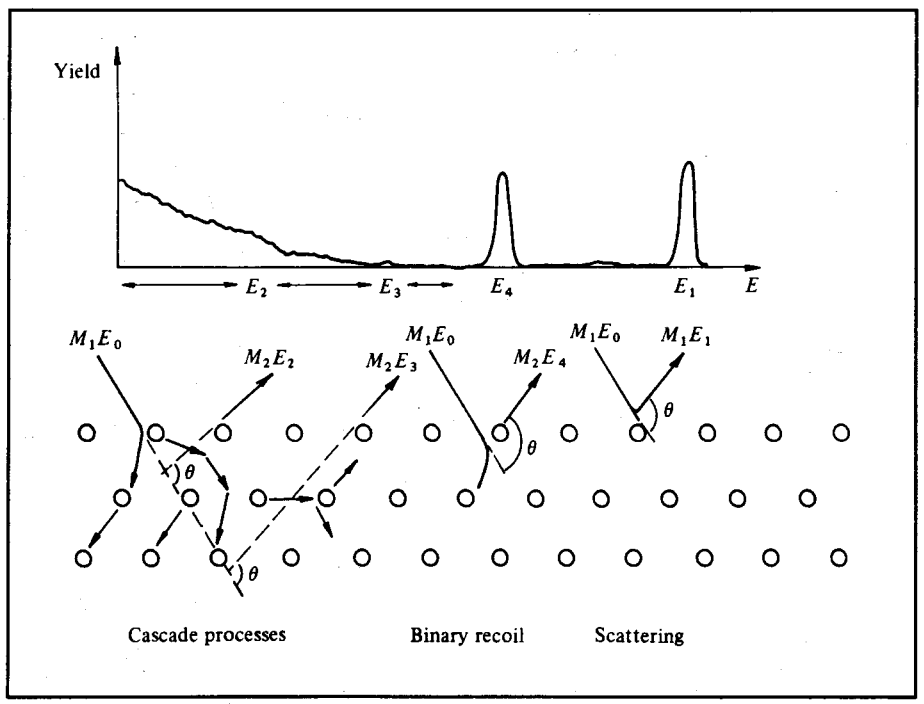

Figure 2.3: Particle ejection processes during ion bombardment and the corresponding energy distribution [WAL89].

Firstly, an incident ion can knock a surface atom out off the surface, these atoms are know as recoil atoms or recoil ions in case they are ionized. The energy of the recoil particles can be calculated from equation 2.2.

$$E=E_0\frac{4q}{(1+q)^2}\cos^2\theta \qquad (2.2)$$

Because this is the result of a single collision it is only in the forward direction that recoil atoms will be detected. This means that for LEIS configurations with $\theta > 90^\circ$, as is the case for the EARISS apparatus, no recoil particles will be detected.

Secondly, there are sputtered ions which are the result of a collision cascade, see fig. 2.3. Such a collision cascade happens because the target atoms get displaced when hit by the incident ions and, therefore, they can collide with other atoms. As a result particles may be emitted from the surface (see for instance [WALL 89]). Obviously the surface gets damaged by this sputtering process. Therefore, the ion dose has to be kept low enough so that no significant damage to the surface occurs.

Mass resolution

One can only distinguish between different target masses when it is possible to resolve the associated energy peaks. This, of course, depends on the absolute width of the energy peaks and the distance, in energy units, between the peaks. The distances between the peaks depend on the following factors as explained before (see page 10) :

- the scattering angle.
- the primary ion used and it's energy.
- the masses of the surface atoms.

The factors that contribute to the peak broadening include:

- the energy spread of the primary beam.
- the spread in the scattering angle.
- the analyzer energy resolution.
- inelastic losses in the scattering process.
- thermal broadening caused by the vibration of target atoms. This influence is largest for a scattering angle of 180°. In that case, the thermal peak broadening ΔE_{vibr}, is equal to [HEL86],

$$\Delta E_{vibr} = 8\frac{q-1}{(q+1)^2}(qE_0E_{vibr})^{1/2} \qquad (2.3)$$

Where E_{vibr} is the vibrational energy of the surface atoms (0.025 eV at room temperature).

2.3 Quantitative ion yield

The yield of the scattered ions from the surface can be written as a product of several factors:

$$Y = N\,C(E)I\delta(E)P^{+}(E)\Delta\Omega \qquad (2.4)$$

Where :

N is the atomic density.

C(E) is a instrument dependent factor.

σ(E) is the differential cross section.

P^{+}(E) is the fraction of ions that doesn't get neutralized.

I is the target current.

$\Delta\Omega$ is acceptance angle of the analyzer.

In order to perform a quantitative analysis of the surface composition the relationship between the atomic density N of an atomic compound and the scattering yield has to be known. Therefore, the factors in equation 2.3 have to be know. The target current I, the acceptance angle $\Delta\Omega$ and the yield are known. This leaves the machine dependent factor C(E), the scattered ion fraction $P^+(E)$ and the cross section $\sigma(E)$ to be determined.

The machine dependent factor can only be determined experimentally and depends on the energy. The two remaining factors also depend on the type of incident ions used and the kind of target atoms. The differential cross section can be calculated from the interatomic repulsive potential. With good success screened coulomb potentials,

$$V(r)=\frac{Z_1 Z_2 e^2}{r}\phi(r) \qquad (2.5)$$

have been used, using the Moliere approximation to the Thomas-Fermi potential, for the screening function $\phi(r)$.

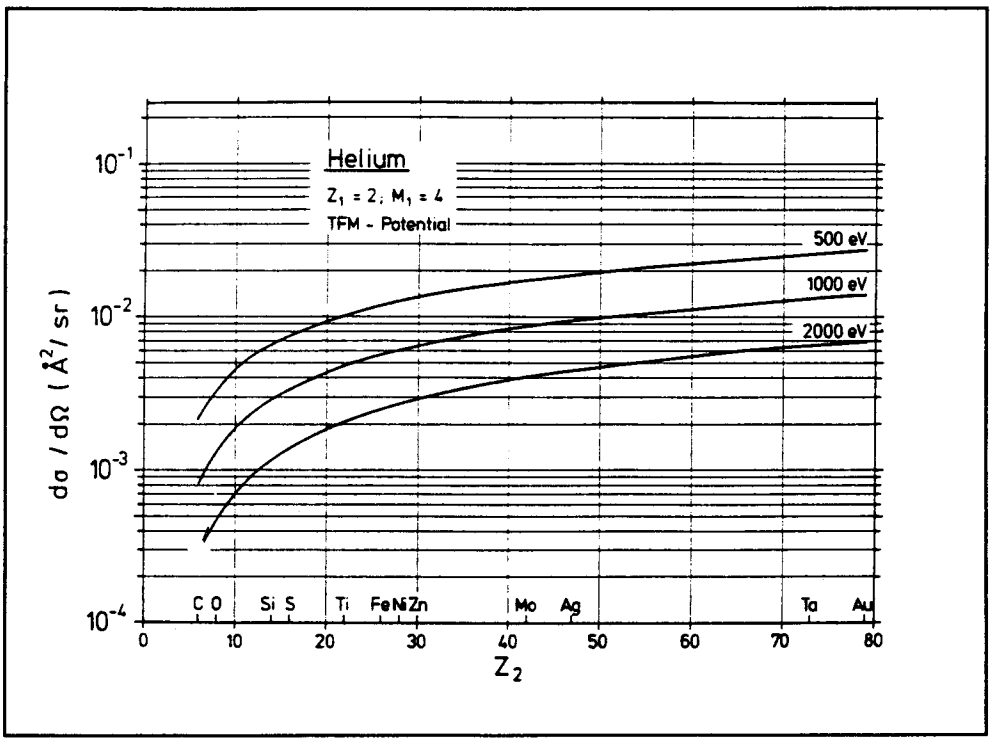

Figure 2.4: Calculated dependence of the scattering cross-section on the target atomic number for three different primary energies. The scattering angle is 137° [TAG85].

In fig. 2.4 this is illustrated by showing the dependence of the cross section on the target mass for three different energies. In fig. 2.5 the measured ion yield for several elements is shown [TAG85].

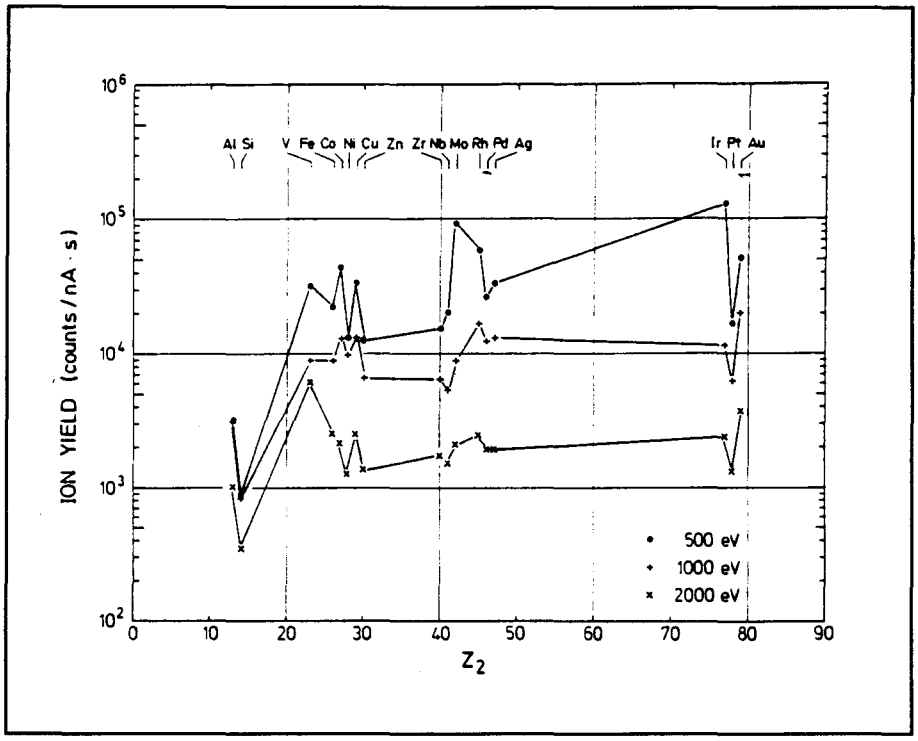

Figure 2.5: Yield of He^+ ions scattered from various elemental surfaces. The data was taken with a cylindrical mirror analyzer (θ = 137°) at three different primary energies [TAG85].

Comparison with fig. 2.4 shows that the general behaviour can be accounted for by the cross section. However, there are substantial variations around this dependence because only ions will be detected. This underlines the importance of the neutralisation effect which gives rise to the factor $P^+(E)$. The principles of the basic neutralisation processes namely Auger and resonance neutralisation, are quite well known [HAG54].

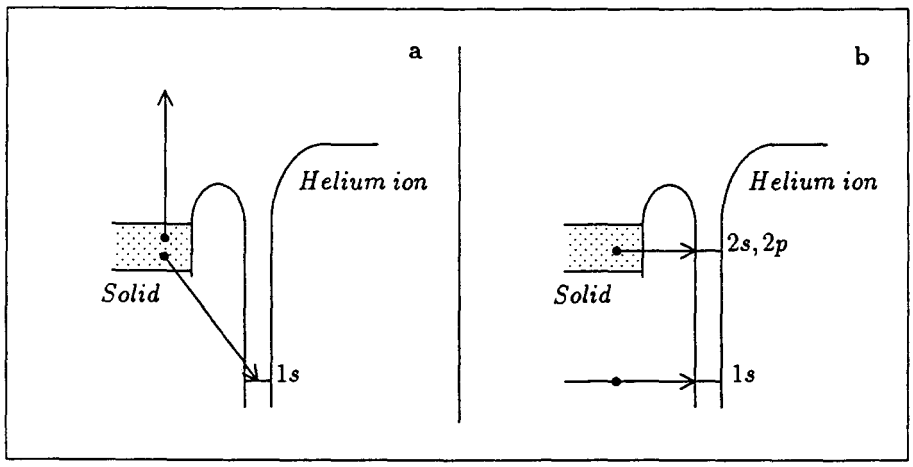

Figure 2.6: Schematic illustration of the Auger neutralization process (a) and the valence and core level resonance neutralization process (b) [ACK90].

In the Auger neutralisation process (fig. 2.6a) the vacancy in the He^+-1s energy level is filled by an electron from a higher level of the solid. The energy difference between the two levels is consumed by another electron which emits from the solid. In the resonance neutralization process (fig. 2.6b) an electron of the solid can be transferred without energy loss if its energy corresponds to a vacancy level of the He^+ ion.

For constant angles of scattering and incidence, Brongersma and Buck [BRO76] have shown that $P^+(E)$ could be written as,

$$P^+ = e^{(-\frac{a}{v_f})} \tag{2.7}$$

a is the neutralisation constant and v_f is the velocity of the ion after scattering. According to (2.5) the ion fraction P^+ should depend smoothly on the energy however this is not always true, see for instance Erickson and Smith [ERI75].

Because no neutralisation models exist that are detailed enough to determine the value of the neutralisation constant, the ion fraction P^+ can only be determined by calibration measurement. This can be done by using single element samples as calibration samples. A new calibration technique, the DISC method [ACK90] which is based on the comparison between spectra taken with $^4He^+$ and $^3He^+$ under the same experimental conditions has been successfully used.

A way to circumvent this neutralisation dependence is the use of alkali ions which have ion fractions P^+ close to one. The drawback of this is that the information depth increases so that several atomic layers will contribute to the energy spectrum. This greatly complicates the interpretation of the energy spectrum.

2.4 Structural Analysis

Shadowing and blocking

Shadowing and blocking effects can be used to relate scattering intensities to the atomic configuration of the target atoms. To explain this principle we will first introduce the concept of the shadow cone, see fig. 2.7.

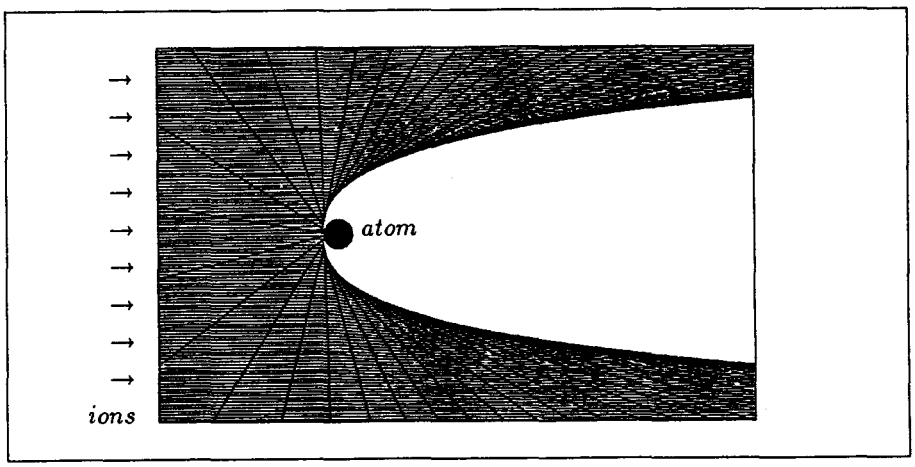

Figure 2.7: Schematic sketch of the shadow cone behind an atom [ACK90].

For this figure a large number of possible trajectories have been calculated for an ion that collides with a surface atom. Behind the target atom we see that there is a region were no ion can come, the so-called shadow cone. The shape of this shadow cone depends on the interaction potential between the ion and the target atom, see equation 2.5. As can be seen from fig. 2.7 there is a high density of trajectories at the edge of the shadow cone this focusing effect intensifies the edge of the shadow cone. When an atom lies in the shadow cone of another atom it can not be seen as is illustrated in fig. 2.8.

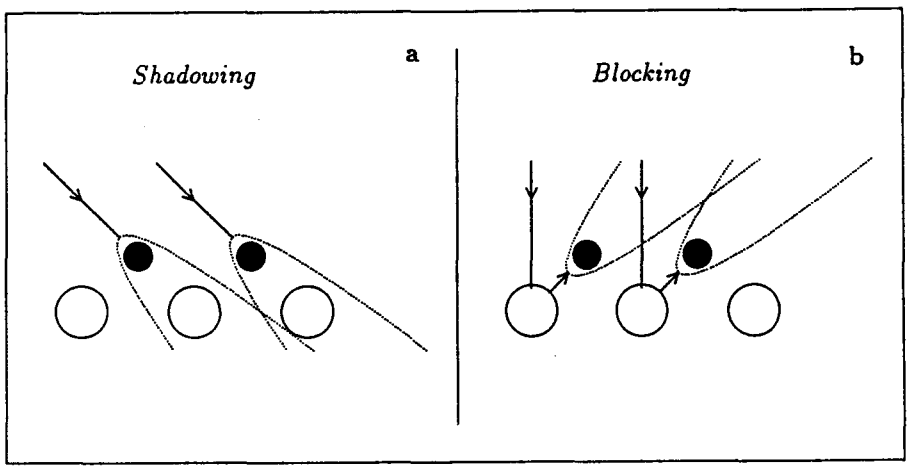

Figure 2.8: Schematic representation of shadowing and blocking effects.

By varying the angle of incidence of the primary beam or rotating the target azimuth the atom can be shifted out of the shadow cone and made to contribute to the scattering yield. This transition is enhanced by the focusing effect at the edge of the shadow cone The blocking effect, see fig. 2.8b, prevents ions to reach the detector under certain scattering angles and for certain azimuthal angles. If we assume the angle of incidence and scattering to be fixed, as is the case for the EARISS configuration, we can obtain information about the surface structure by looking at the scattering yield of the white atom in fig. 2.8b as a

function of the azimuth.

Multiple scattering

Another structure related effect that can be used to study the surface structure is based on multiple scattering. When an ion is scattered over a certain angle as a result of two collisions its energy loss will be less than that of an ion that collided only once. Therefore, we can distinguish between these two processes in the energy spectrum. At grazing angles of incidence with respect to the surface and low scattering angles, double collisions will occur more often in those surface directions were the target atoms are more closely packed and so a higher scattering yield will be found for these directions. Because of the high neutralisation probability of noble gas ions the ion fraction for double collisions will be very low. Only if one uses Ne^+ ions and special LEIS configurations the ion fraction for double collisions becomes large enough to be detected. Also if one can detect neutrals as well as ions the multiple scattering peaks can be seen, this is for instance the case in time of flight measurements.

Chapter 3

The EARISS apparatus

3.1 Introduction

One of the major concerns in LEIS is the damage to the surface due to the incident ions. Therefore, the ion dose has to be kept to a minimum during LEIS experiments. To make a much more efficient use of the scattered ions than conventional LEIS equipment the EARISS apparatus is being developed at the Eindhoven University of Technology in the Surface Physics Group. The reason for the much higher efficiency is the simultaneous detection of the energy and azimuthal distributions. This eliminates the need for energy scans and measuring of spectra at a large number of different azimuthal angles. From the energy distribution the compositional information of the surface is obtained and from the azimuthal distribution the structural information.

In this chapter a brief description of the EARISS set-up will be given. More detailed information has been given by Hellings [HEL86], van der Meulen [MEU88] and Ackermans [ACK90]. Recently the primary ion source has been replaced and the sample manipulating system has been improved.

3.2 The Analyzer

The principle of the EARISS is shown in fig. 3.1.

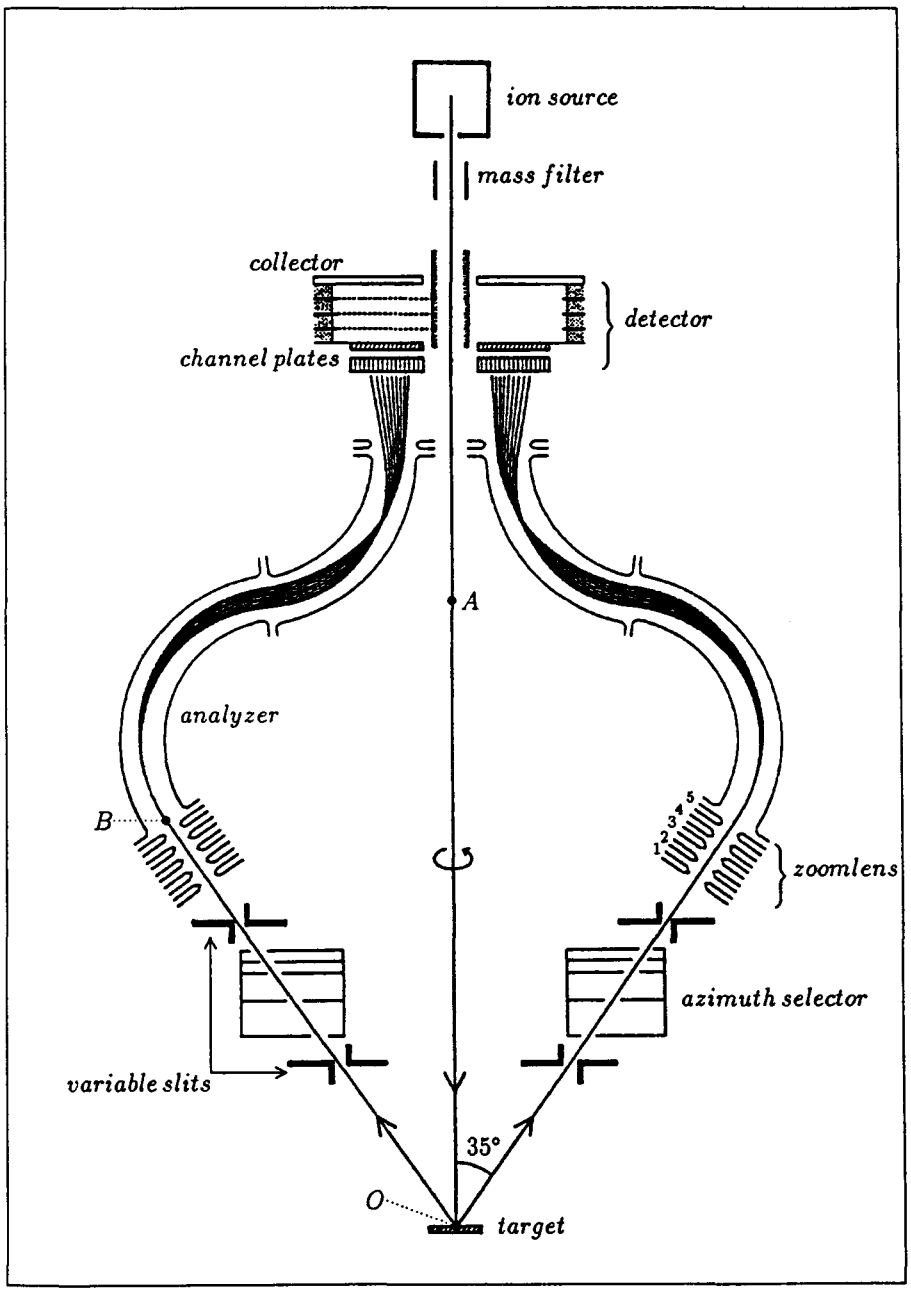

Figure 3.1: Schematic representation of the EARISS analyzer. As an indication of the dimensions: the distance from point B to the central axis is about 78 mm [ACK90].

The primary ions are directed perpendicular onto the surface. Only ions which are scattered through 145° are accepted by the opening of the entrance slit. A double toroidal analyzer has been designed by Hellings et al. [HEL85] in such a way that the energy distribution is displayed linearly along the radius of the detector. Ions with low energies will be projected at large radius and those with high energies near the central axis. The analyzer only accepts ions within 6% of its pass energy. This pass energy can be varied by changing the voltages applied to the analyzer. In this way the size of the energy window can be chosen. One can chose either a small energy window to obtain good energy resolution or a large energy window to image a large part of the energy spectrum at once. The position of this energy window within the energy spectrum can be set by an accelerating section with focusing elements ("zoomlens") at the entrance of the analyzer. The energy displaced in the middle of the energy window is simply given by:

$$E_m = E_{pass} + qV_3 \qquad (3.1)$$

Where E_{pass} is the pass energy and V_3 is the accelerating voltage.

One problem is still that the azimuthal velocity of the ion is preserved in the analyzer. This means that many of the ion trajectories don't lie in the meridian plane (plane AOB in fig. 3.1) but that a spiralling path will be followed. This decreases, of course, the azimuthal resolution considerably. Ackermans [ACK90] has estimated the azimuthal resolution to be ~ 94°. The construction of an azimuth selector, as indicated in fig. 3.1, which prevents spiralling paths to occur is currently under construction.

3.3 The variable slits

In order to be able to narrow the spread in the acceptance angle of the analyzer the EARISS apparatus is equipped with a unique feature, the variable slits, see fig. 3.2 .

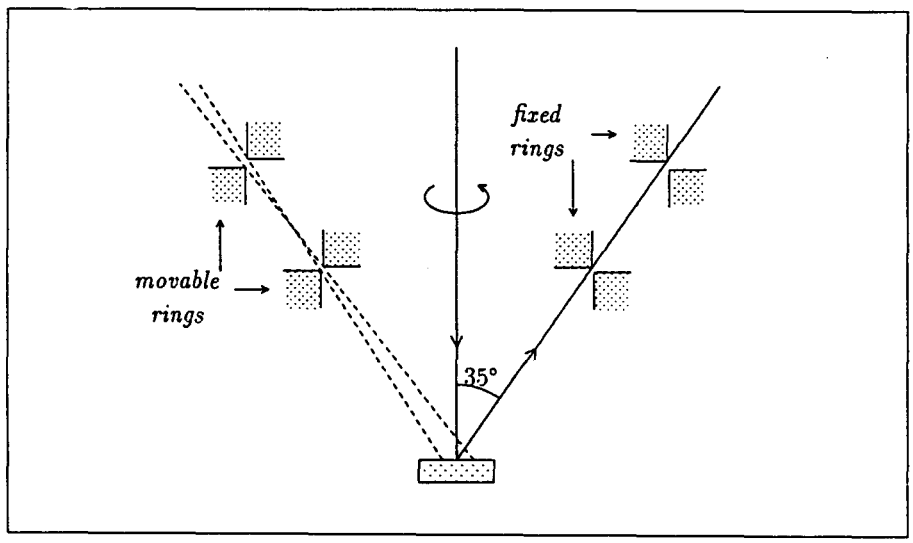

Figure 3.2: Principle of the variable slits. The two inner rings are fixed to the analyzer. The two outer rings can move vertically [ACK90].

These slits can be operated from outside the vacuum system. This gives the possibility to chose between high energy resolution or high signal. Each of the two slits consists of a ring that is fixed to the analyzer and a ring that can be moved upward and downward, see fig. 3.2, which causes a change in the spread of the acceptance angle. The maximum spread in the acceptance angle is 3.27°. Reducing the acceptance angle also reduces the spot size at the target from which ions are accepted by the analyzer, as is indicated in fig. 3.2.

3.4 The Detector

When an ion has passed the analyzer its charge has to be amplified to obtain a measurable signal. This has to be done without losing the position with which the ion left the analyzer because this position contains the energy and azimuthal information. To achieve this a cascade of two channelplates is used as can be seen in fig. 3.3. A hole has been made in the middle of these channelplates to allow the primary beam to pass through.

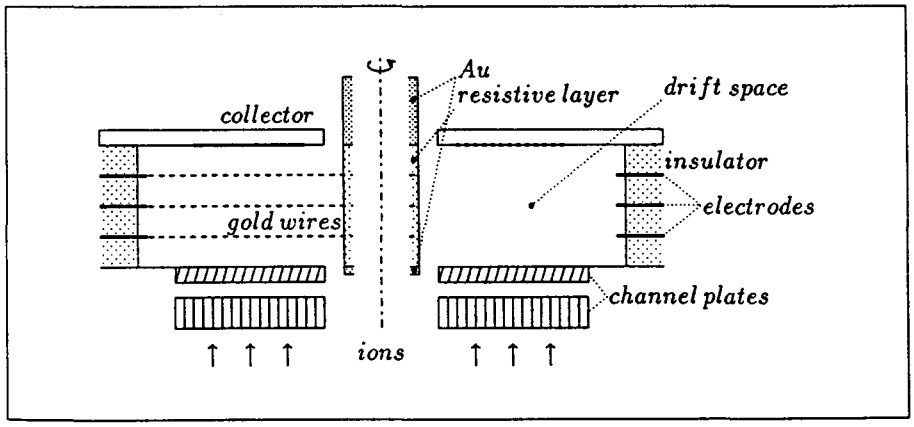

Figure 3.3: Schematic cross-section of the detector unit (not to scale) [ACK90].

A channelplate is a thin glass plate containing a large number of channels (approximately 10^6 channels), see fig. 3.4. The channels have a diameter of 12.5 μm each. The channelplates have an inner diameter of 20 mm and an outer diameter of 46 mm. The first channelplate is 1 mm thick and the second one is 0.5 mm thick.

The inside of a channel is coated with a slightly conducting material. A high voltage, typically 1 keV is applied over the channelplates. When a particle hits the wall of such a channel an avalanche of secondary electrons is triggered as illustrated in fig. 3.4.

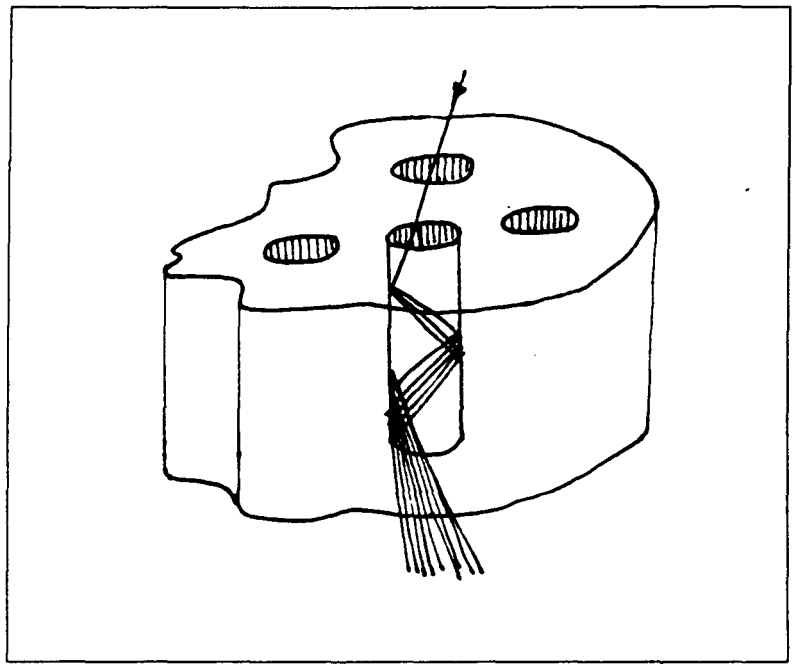

Figure 3.4: Electron multiplication in a channel of a channelplate.

This gives an amplification of the order of 10^3 per channelplate. When we put two channelplates in series, as in our case, the resulting overall amplification is about 10^6. The second channelplate is operated in the so called space charge saturated mode. This means that the electron clouds leaving the second channelplate show a characteristic size. We take advantage of this when discriminating between signal and noise, see section signal processing. Because the amplification occurs via narrow channels the positional information of the ion is preserved.

A problem which occurs in channelplates is the ionisation of the residual gas by the electrons. Generated ions can be accelerated back into the channels and also cause an avalanche of secondary electrons. To reduce this so called ionic feedback the channels of the second channelplate make an inclination of 13^0 with the surface normal. This limits the penetration depth of the ion and, therefore, also the magnitude of the avalanche.

The charge collector on which the electron clouds fall must be position sensitive.

To illustrate how this position sensitivity is obtained, we first discuss a simple 1 dimensional case, as illustrated in fig. 3.5a.

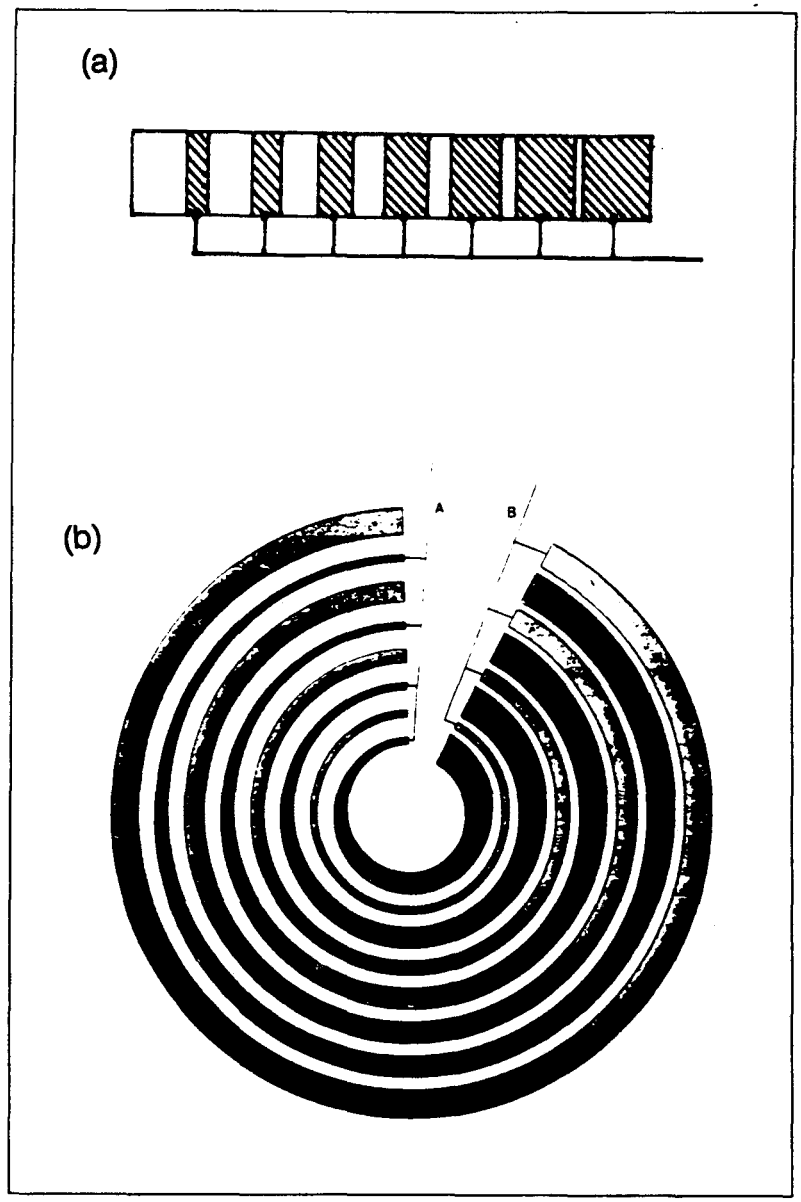

Figure 3.5: Position sensitive collector strip pattern (a) for a simple linear detector (b) for a two dimensional (r.φ)-detector [KNI87].

This detector consists of several strips that increase in width from left to right. The distance between the right boundaries of the strips are equal. All the strips

are electrically interconnected. If an electron cloud is large enough to cover several strips, its position can be obtained from the measured charge when the total charge is known. The two-dimensional EARISS detector is based on the same principle, see fig. 3.5b.

One set of strips has an increasing width along the radius, the other set along the azimuth. We will call these strips the E-strips and the ϕ-strips, respectively.

The collector plate is a glass substrate with golden strips on top and a conducting backplane, a cross section is shown in fig. 3.6.

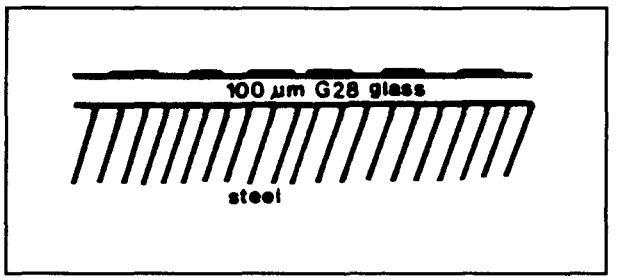

Figure 3.6: Cross-section of the collector. The collector consists of thin gold strips deposited on a glass substrate which is mounted a steel support.

In total there are 14 E and 14 ϕ-strips with conducting shielding strips in between adjacent strips.

The purpose of the shielding strips and the backplane is to minimize the cross talk between the E and the ϕ-strips. Therefore, the shielding strips and the conducting backplane have to be coupled to ground. Because the collector is put at a high voltage they are AC coupled to ground by a capacitor. In fig. 3.7 we illustrate this by showing a simplified scheme of the charge collector and the preamplifiers.

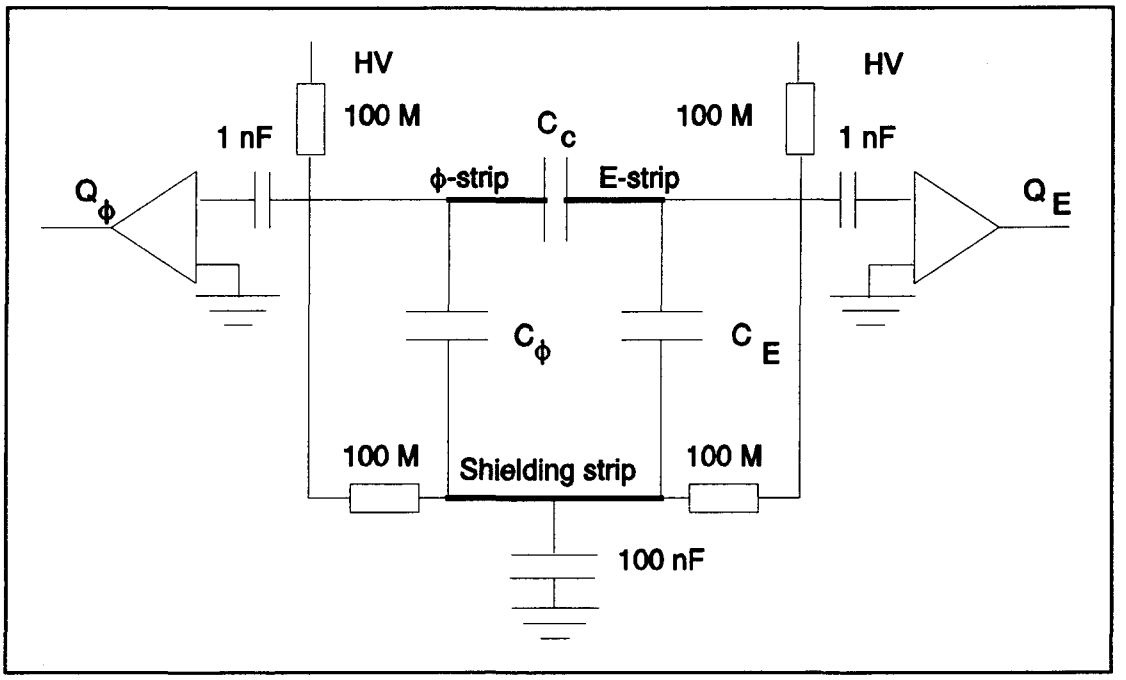

Figure 3.7: Simplified scheme of the charge collector and the preamplifiers

The capacitors C_E and C_ϕ represent the capacitance between the E the ϕ and the shielding strips. C_c is the coupling capacitance between the E and the ϕ-strips. For more details we refer to v/d Meulen [MEU88].

Besides the two signals obtained from the collector plate a third signal which is a measure of the total charge of the electron cloud is obtained from the sum of the charge losses of the front and the back of the second channelplate when releasing a charge cloud. By normalizing the signals from the collector plate with the signal obtained from the second channelplate measures for the energy and azimuth are obtained.

3.5 Signal processing

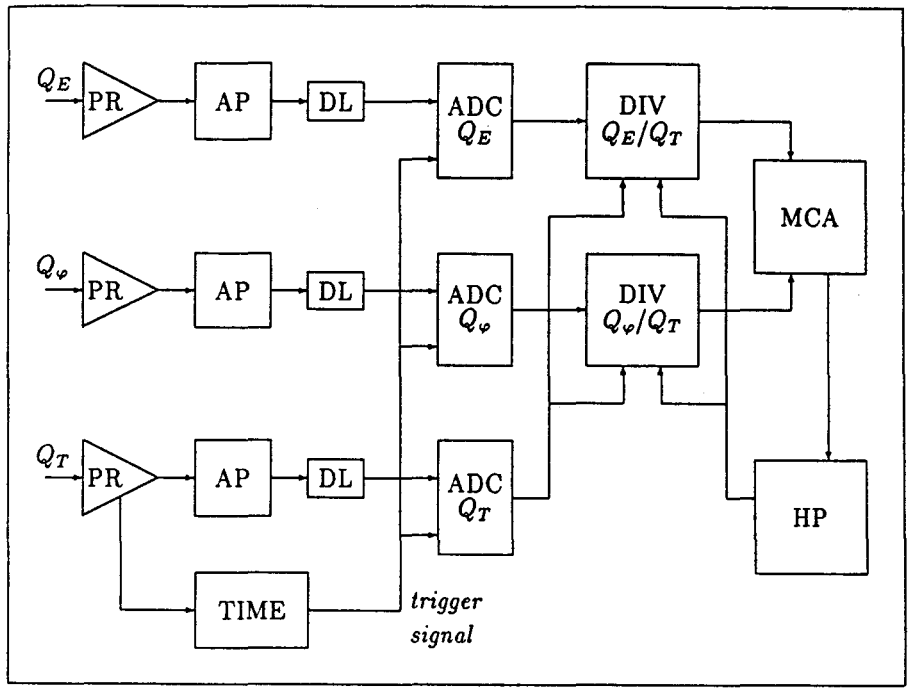

Figure 3.8: Schematic representation of the data processing system of the EARISS apparatus. The components are: preamplifiers (PR), amplifier and pulse shapers (AP), variable delays (DL), analog-to-digital converters (ADC), divider memories (DIV), multichannel analyzer (MCA) and the HP9000/330 computer (HP) [ACK90].

Three signals are obtained by the EARISS apparatus when an ion is scattered off the surface. That is two signals from the collector plate which we will call Q_E and Q_ϕ and one from the second channelplate which will be called Q_T. While these signals are processed all other scattering event will be neglected. This so-called dead time is about 1.5 μs. A scheme of the signal processing is shown in fig. 3.8.

Analog circuit

Q_E, Q_ϕ and Q_T are first amplified by charge sensitive amplifiers, (Canberra 2006 for Q_E and Q_ϕ and Canberra 2003BT for Q_T). The charge sensitive amplifier for Q_T also generates a fast timing pulse. The height of these output pulses is proportional to the amount of the input charge. Next these pulses are amplified again and pulse shaped by Canberra 2110 timing filter amplifiers. Delay lines are used to delay the pulses to make the trigger signals for the ADC's coincide with the maximum of the pulses. The height of the pulses are then sampled by 8 bit ADC's (Analog Devices, MATV-0811).

The trigger signal is derived from the fast timing pulse of the Canberra 2003BT by a timing circuit. Besides this it also generates a dead time during which no pulses are accepted. Furthermore because, the height of the timing pulse is also proportional to the size of the electron cloud, a discriminator window is used which can separate the signal from amplifier noise.

Digital circuit

The three signals are now converted to 8 bit integers. The next step is to normalize the E and ϕ signals. This is done by dividing Q_E and Q_ϕ by the signal for the total charge Q_T.

$$E=\frac{Q_E}{Q_\phi} \tag{3.2}$$

$$\phi=\frac{Q_\phi}{Q_T} \tag{3.3}$$

There are two ways to perform an integer division. The most straightforward way is the software division where the result is computed with a microprocessor. However, this takes a lot of processing time which reduces the number of scattering events per second, that can be processed. Therefore, we chose a

much faster option, a hardware divider. Here, the two integer divisions are performed by using a look up table which contains all the answers for the possible combinations of numerator and denominator. The two results combined correspond to an address of a register in a MCA (multi channel analyzer). This register is incremented by one every time the corresponding (E,ϕ)-event occurs. At the end of a measurement the MCA memory is read by a HP 9000/300 computer. By using the available software the data can be displayed graphically. In order to perform measurements when the before mentioned "hardware divider" is out of order, a by-pass by means of a software division is possible. In this case the HP9000/300 reads out the ADC's, performs the division and fills the MCA memory at the end of the measurement.

3.6 The vacuum system

In this section we will only give a very short description of the vacuum system. For more details we refer to v/d Meulen [MEU88]. A cross section of the vacuum system is shown in fig. 3.9 (see next page). The primary ion source is mounted on the top of the vacuum chamber. The principle is as follows: the ions are made in an ionisation chamber where electrons emitted from filaments ionize the gas. These ions are then extracted from the ionisation chamber by an extraction potential and are guided via a system of deflection plates and focusing elements onto the target. A Wien type of mass filter is placed in the beam. This gives a relative mass separation $\Delta M/M$ of about 10% [HEL86]. For the measurement on Ni(100) as presented in this thesis a home built ion source was used. After these measurements the ion source was replaced by a Leybold IQE12/38 ion source. This ion source is currently still in use.

Besides the primary ion source a second ion source which makes an angle of 20° with the target surface (when it is in a horizontal position) is mounted on the vacuum chamber. Together with a drift tube on the other side of the vacuum chamber it is used to perform time of flight measurements. A third surface analytical technique which is directly available is a small Low Energy Electron

Diffraction (LEED) apparatus

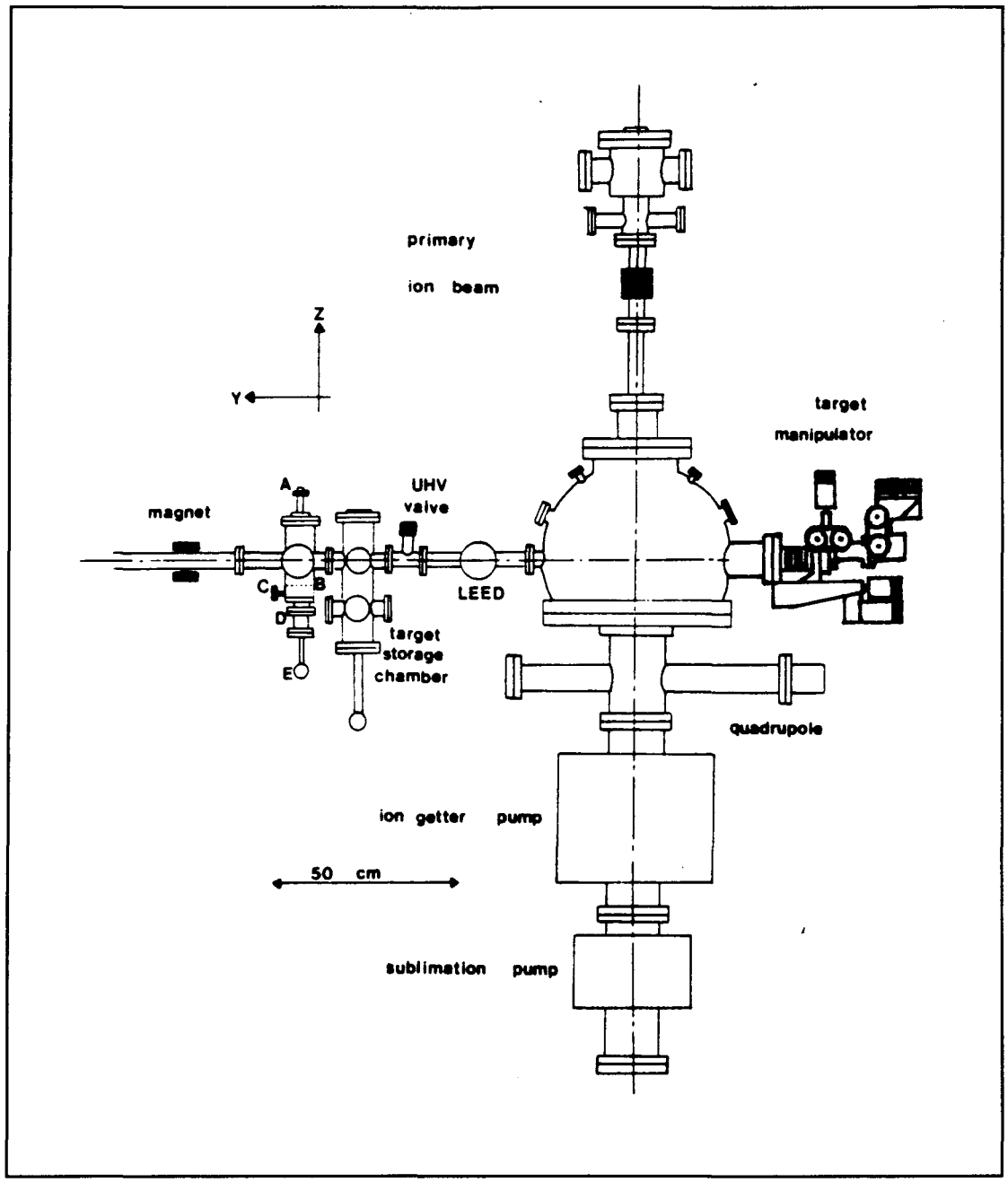

Figure 3.9: Cross-section of the EARISS apparatus [ACK90].

The sample is mounted on a modified Panmure Instruments Ltd. manipulator [WIL90] which has six independent movements. For sample preparation the sample can be heated in situ with a Riber TUM D10 oven. Furthermore a sputter ion gun for cleaning the sample is mounted on the vacuum chamber.

In order to make quick exchange of samples possible the EARISS apparatus is equipped with a target storage chamber which can contain up to seven samples. Other samples can be introduced via a loadlock.

UHV conditions are achieved by the use of a turbo molecular pump, several ion getter pumps and two titanium sublimation pumps. For the measurement in this thesis we were content with a base pressure of 3. 10^{-9} mbar. With extra effort it is possible to enter the 10^{-10}-10^{-11} mbar range, as has been shown in the past. The analysis of the residual gas is done by a Balzers mass spectrometer (QMS311 with a QMA410 analyzer).

Chapter 4

Imaging characteristics of the EARISS apparatus

4.1 Introduction

The EARISS-apparatus is capable of measuring the energy and azimuth with which an ion is scattered off the target. This information is transformed into a two-dimensional rectangular image. Along the short side of this rectangle the energy varies and along the long side the azimuth.

The analyzer and detector have been designed to give an image that should be linear in both the energy and azimuth. Also the place and size of the energy window can be calculated based on design parameters, see section 3.2.

Measurements have been performed to study the characteristics of this two-dimensional image and a comparison with the theoretically calculated predictions is made.

4.2 Experiments

For the experiments we chose to use a Ni(100) sample. This is a single-crystal which is expected to show no measurable azimuthal dependence for our LEIS configuration. To illustrate this we show the surface structure for the (100) plane in fig. 4.1.

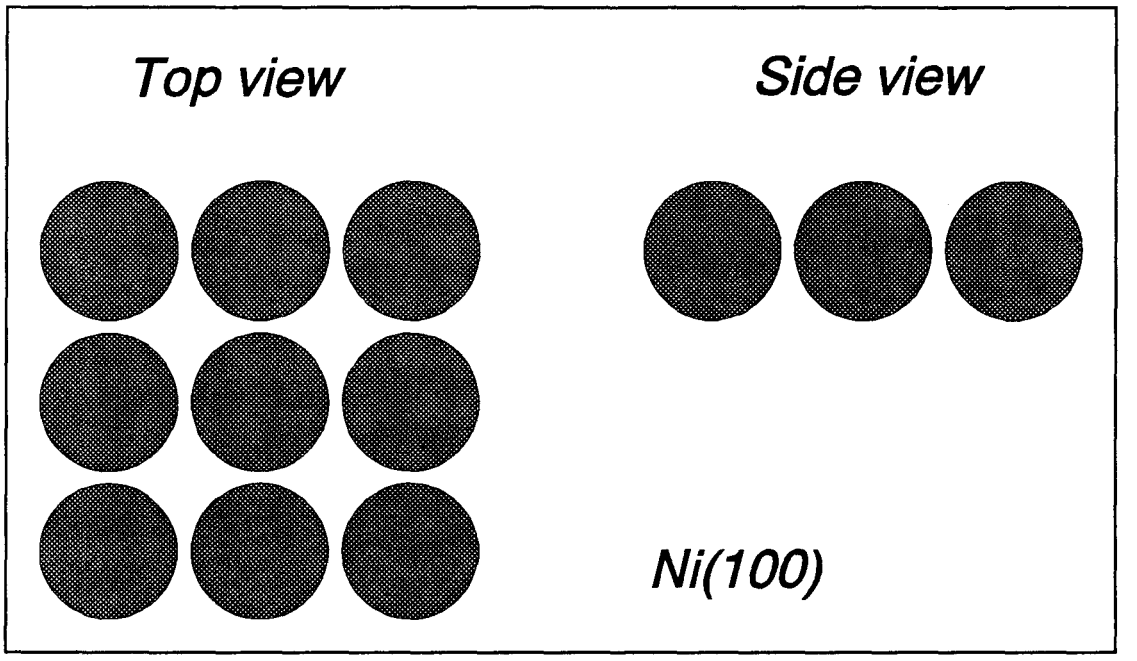

Figure 4.1: Ni(100) surface structure.

As is evident from this figure there are no blocking effects (see section 2.4) that could give rise to variations in the azimuthal distribution.

Cleaning of the Ni(100) sample was done by sputtering with 3 keV Ar^+-ions.

Because the hardware divider was out of order during these measurements, the divisions had to be carried out by using the software division option, see section 3.5. For the countrates used in these experiments,(~ 10^4 c/s), it means that the measuring time has to be increased by a factor of 300 to collect the same number of scattering events. Therefore concessions had to be made with respect to the obtained statistical accuracy.

Unless otherwise indicated the spread in the acceptance angle of the analyzer was set to 2.4° by partly closing the variable slits, see section 3.3, to obtain good energy resolution. All the experiments were done using 3 keV Ne^+ ions. The pass energy was set to 2000 eV, this should give an energy window, based on

calculations, of 240 eV.

4.3 Results and discussion

Fig. 4.2 shows the distribution of the scattered ions from the Ni(100) target.

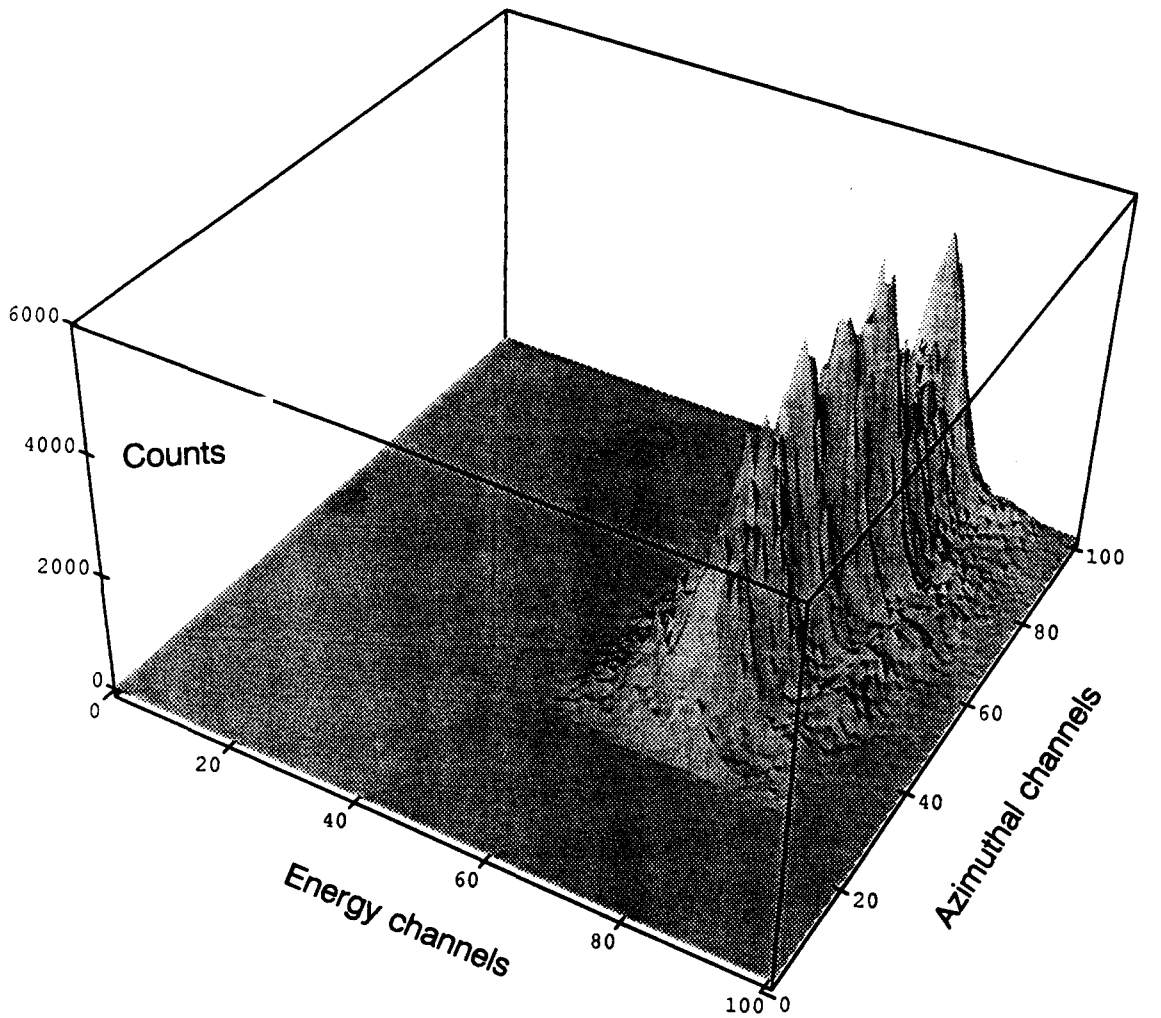

Figure 4.2: EARISS measurement of the Ni(100) surface.

Along the E-axis the energy is displayed and along the ϕ-axis the azimuth. The height is a measure of the number of counts collected for a certain E and ϕ. The spectrum in fig. 4.2 is not rectangular. This is probably caused by the fact that the channels of the second channelplate make an angle of 13° with the surface normal. This causes a displacement of the image on the collector plate which gives rise to the observed S shape. To solve this problem, a third channelplate with straight channels will be placed directly behind the second channelplate in the near future.

Azimuthal imaging capabilities

As noted before, the Ni(100) sample should give a homogeneous distribution along the ϕ-axis. However, this is not the case as is evident from fig. 4.3 which shows the azimuthal distribution.

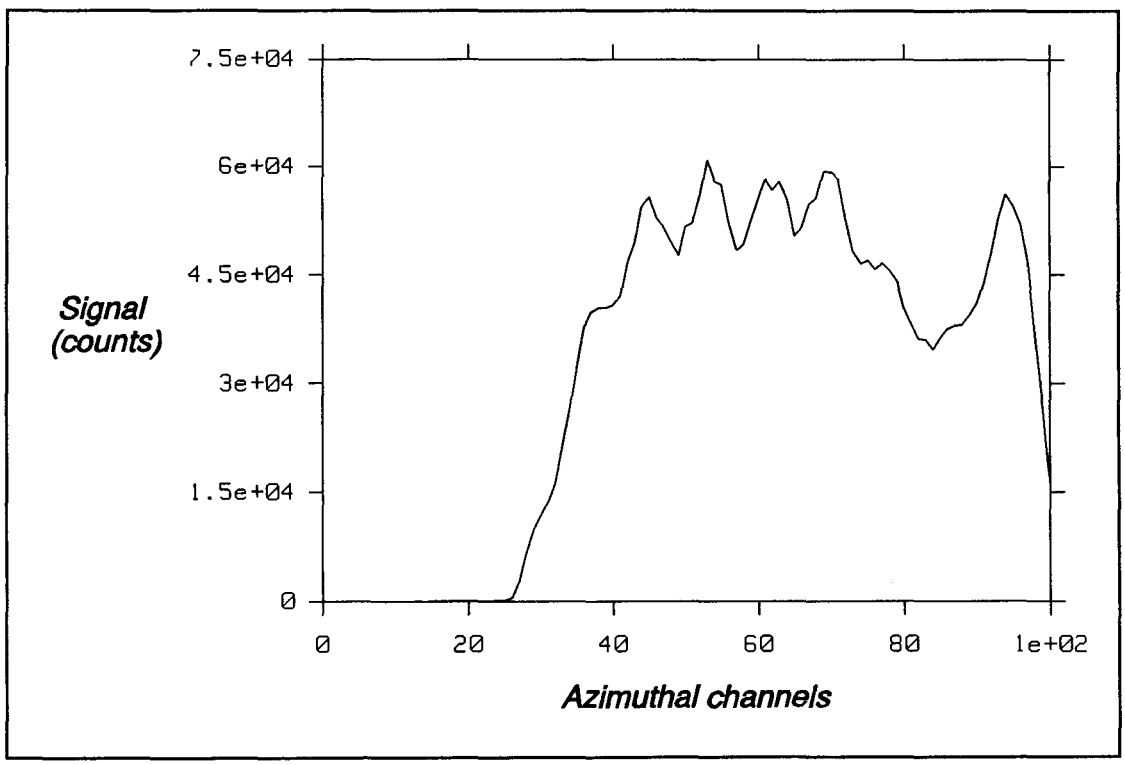

Figure 4.3: *Azimuthal distribution of the Ni(100) measurement shown in fig. 4.2. We have added all the energy channels.*

Two things are characteristic for the azimuthal distribution. Firstly, the dip at channel 85 and, secondly, the apparently periodic peaks. To make sure that this is not caused by the Ni(100) sample we also took spectra where we rotated the Ni(100) sample over 15° respectively 30°. The azimuthal distribution in these measurements are shown in fig. 4.4.

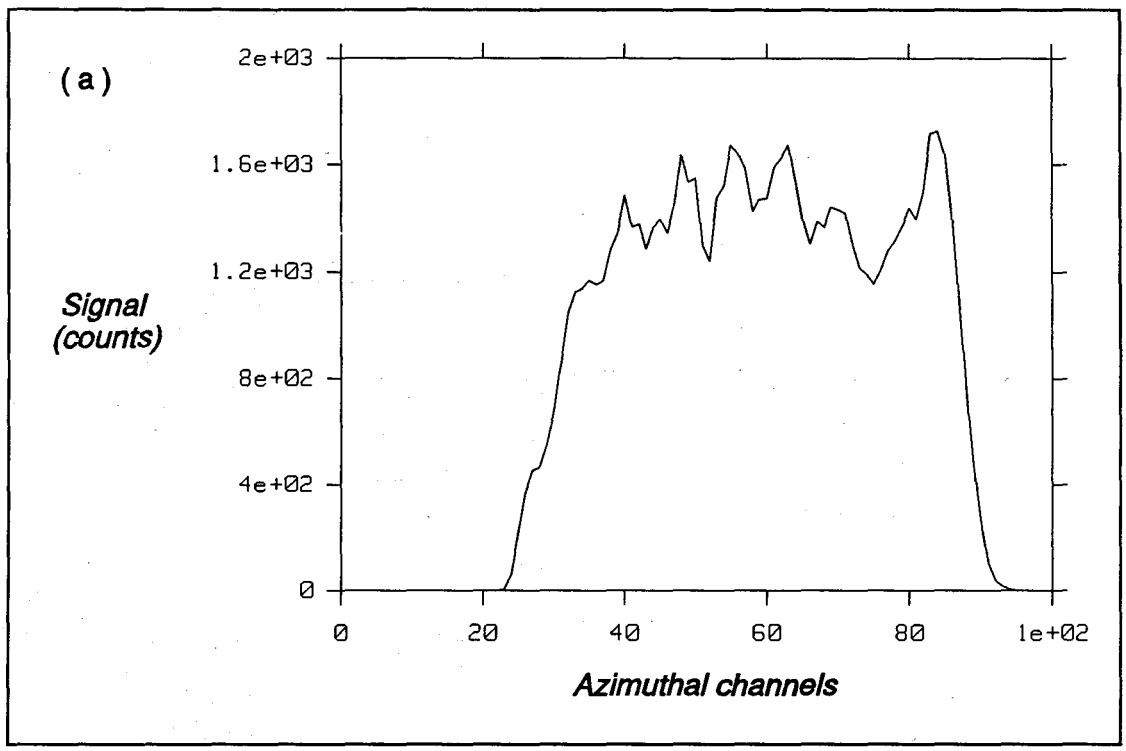

Figure 4.4 a: Azimuthal distributions, measured for a target azimuth of 0° (a).

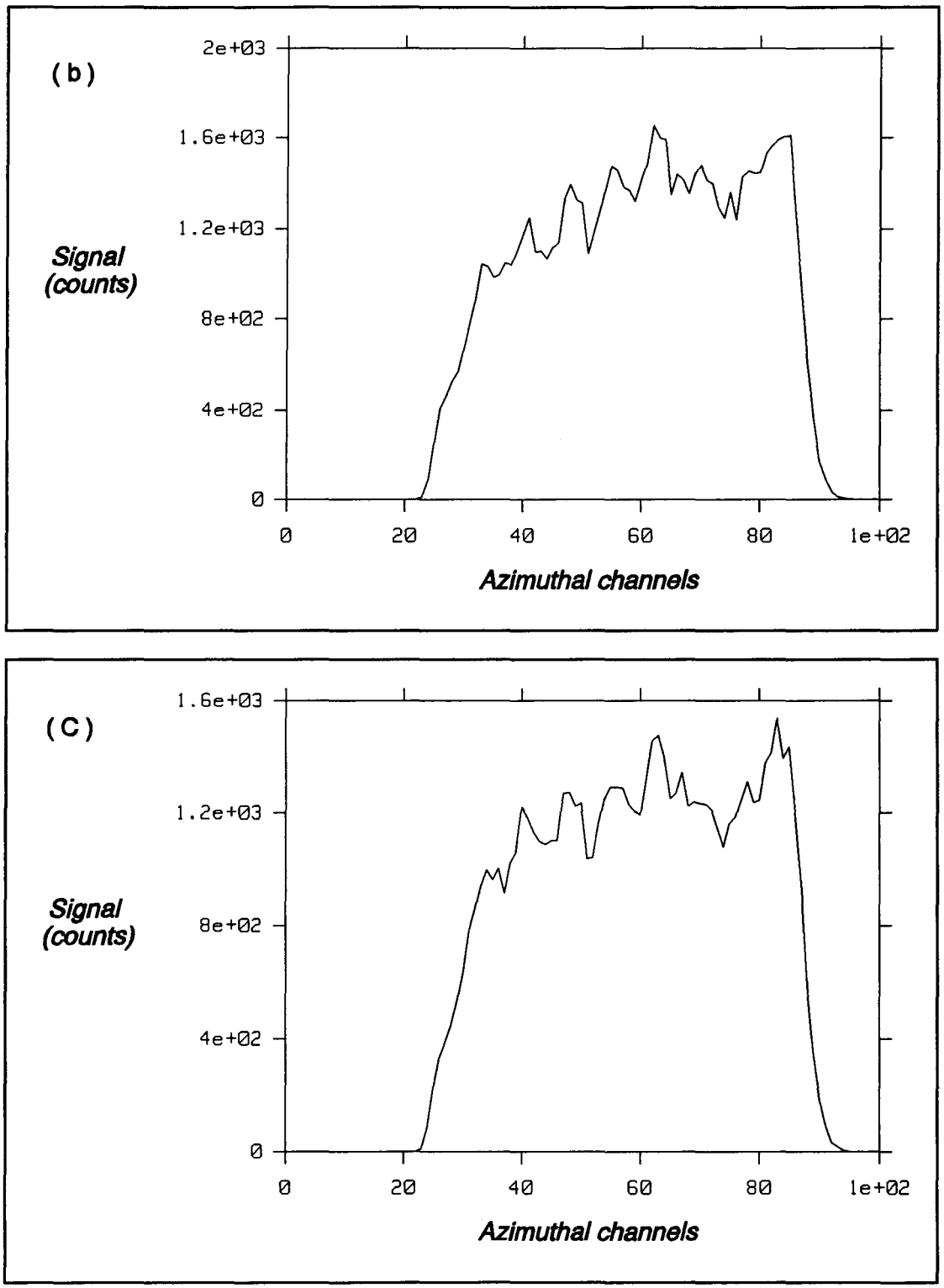

Figure 4.4b/c: Azimuthal distributions, measured for a target azimuth of 15° (a) and 30° (c).

If the variations in the azimuthal distribution are caused by a surface structure related effect, we would expect the peaks to shift when the surface is rotated around its azimuth. However, as can be seen in fig. 4.4, there are no significant changes in the peak positions. This means that azimuthal distribution is probably caused by the EARISS apparatus itself.

Unfortunately, after these measurements, we lost approximately the left half (the lower azimuthal channels) of the azimuthal distribution. The dip around channel 85 appears still to be there. However, until the cause for this loss is clear, one has to be cautious in interpreting the remaining part of the azimuthal distribution. When searching for the reason for this loss, an oxide layer at the entrance slits of the analyzer was discovered and removed. The effect of this on the azimuthal distribution should become clear when the total azimuthal distribution can be obtained again. It is, however, hard to believe that an oxide layer would cause such a specific azimuthal distribution as the apparently periodic peaks. One would expect a more random pattern. The dip, however, could be explained by this.

Another reason why it is unlikely that the surface itself or the oxide layer is the reason of this azimuthal pattern is the azimuthal resolution of the EARISS apparatus. Ackermans calculated the azimuthal resolution to be 94° [ACK90]. Therefore, we would expect to find the reason at the end or after the analyzer. A possibility is inhomogenities in the sensitivity of the channelplates. This could give a reasonable explanation for the dip at channel 85 but it is unlikely that the inhomogenities are so specific as the apparently periodic peaks. As said before the peaks seem to have a periodic pattern. This could suggest an interference effect although there is no obvious reason to explain this. It is evident that this azimuthal distribution should be known when doing structural surface analysis.

Energy imaging capabilities

To study the linearity of the energy axis of the 2-dimensional image the following experiment was carried out. We took spectra for accelerating voltages V3

ranging from 1100 V to 1500 V with steps of 50 ± 5 V, moving the Ni peak through the entire energy window. Fig. 4.5 shows the successive spectra.

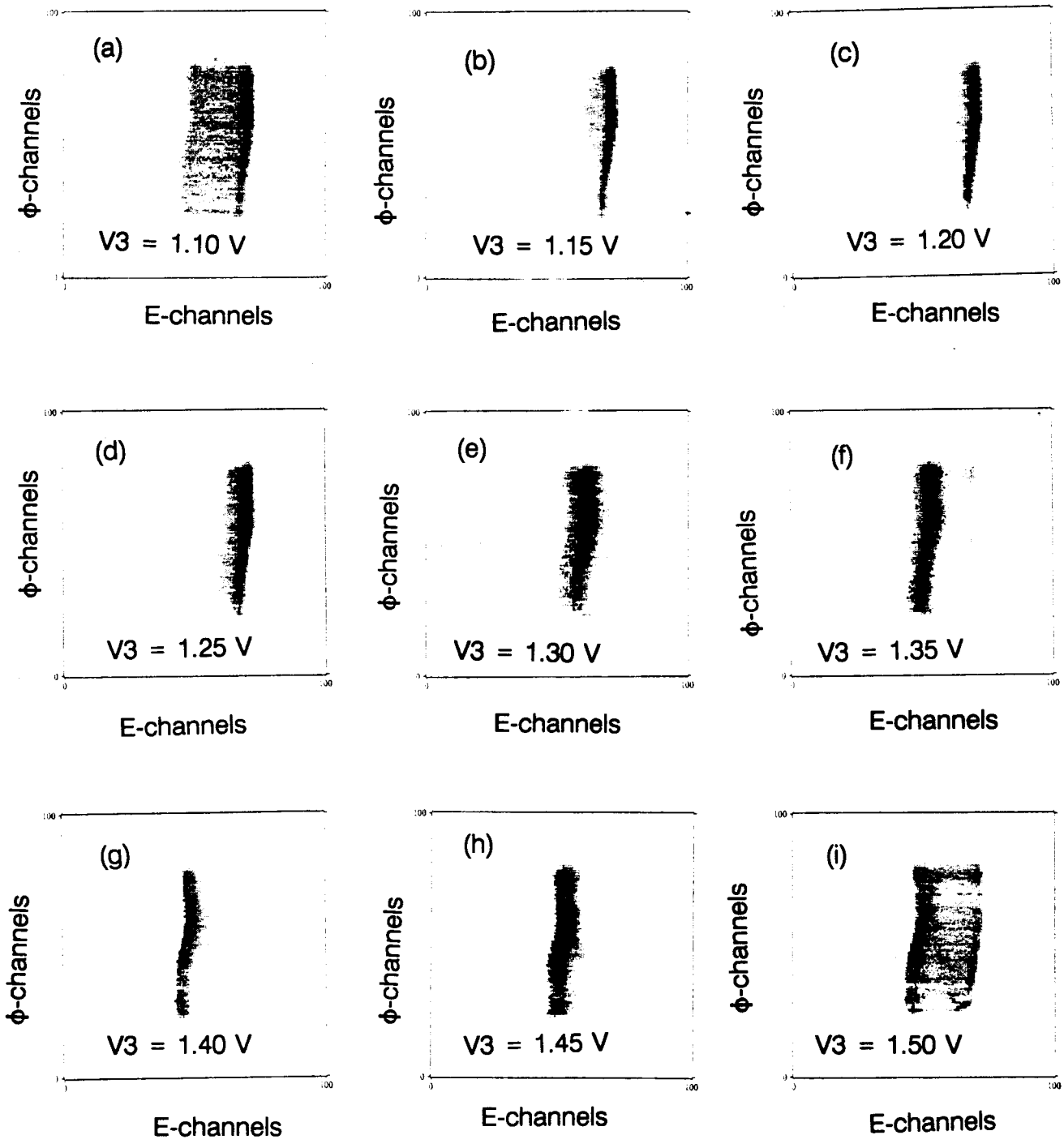

Figure 4.5: Measurements on Ni(100) for accelerating potentials V_3 ranging from 1.10 keV to 1.5 keV with steps of 50 eV.

The displacement within the energy window of the Ni peak as a function of the accelerating voltage V3 is shown in fig. 4.6.

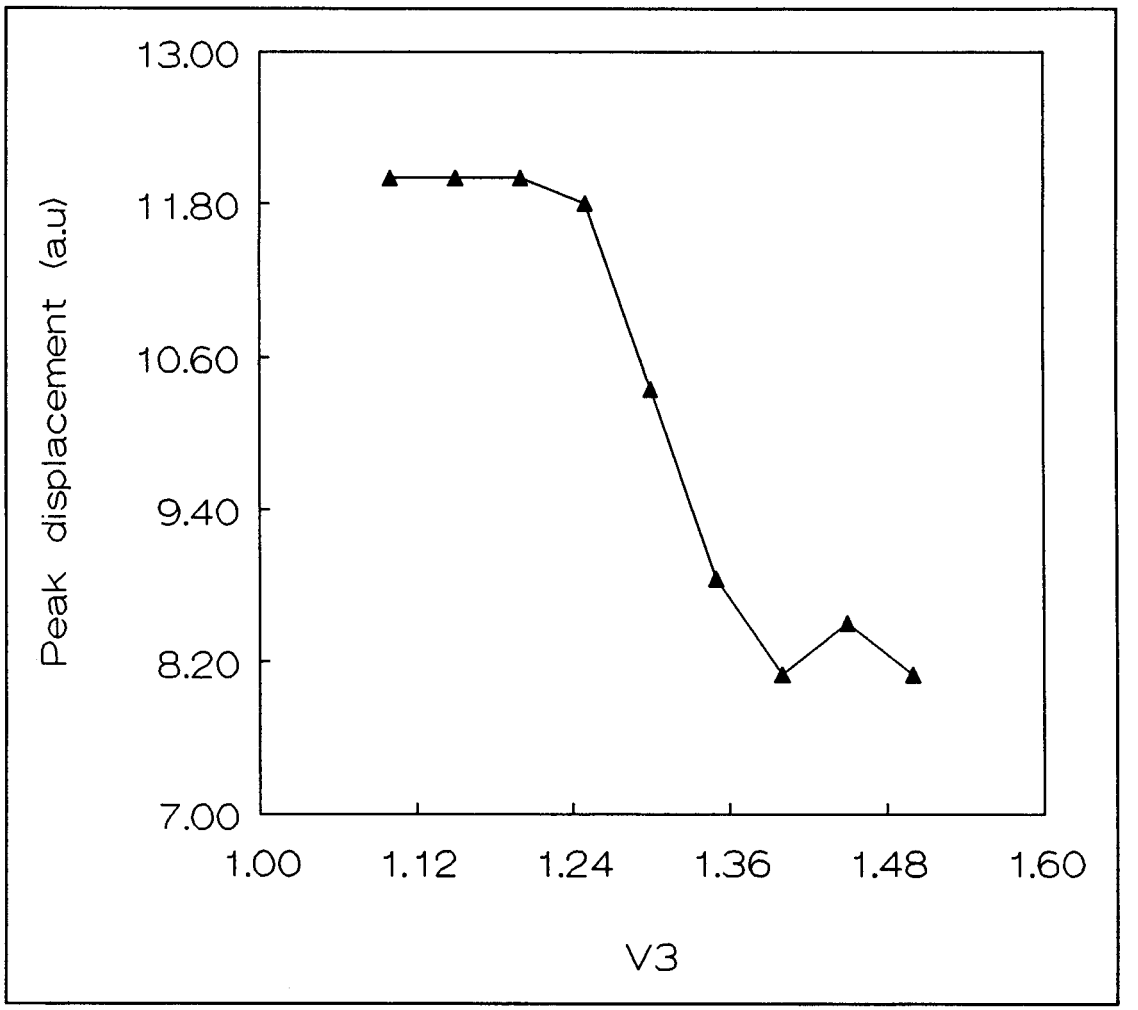

Figure 4.6: Displacement of the Ni peak against the accelerating potential V_3.

Within the energy window the shifts are linear with V3 and, therefore, with the energy. At the edges of the energy window we see that it takes a larger change in V3 to move the Ni peak completely outside the energy window than expected, since the FWHM (Full Width at Half Maximum)of the Ni peak is only 30 eV (see text by

fig. 4.7). Therefore, one has to be sure that the energy peaks lay entirely within

the energy window in order to relate position to energy. Three spectra have a peak that lies clearly inside the energy window, see fig. 4.5. Therefore, these spectra were used to make a calibration between position and energy. From this calibration we calculated the energy window to be 210 eV which is 15% smaller then the calculated width of 240 eV.

Two measures for the energy resolution of the EARISS apparatus have been obtained from the experiments. In fig. 4.7 the Ni peak is shown, this is a cross section of the two-dimensional image where we have added the azimuthal channels 68 and 69.

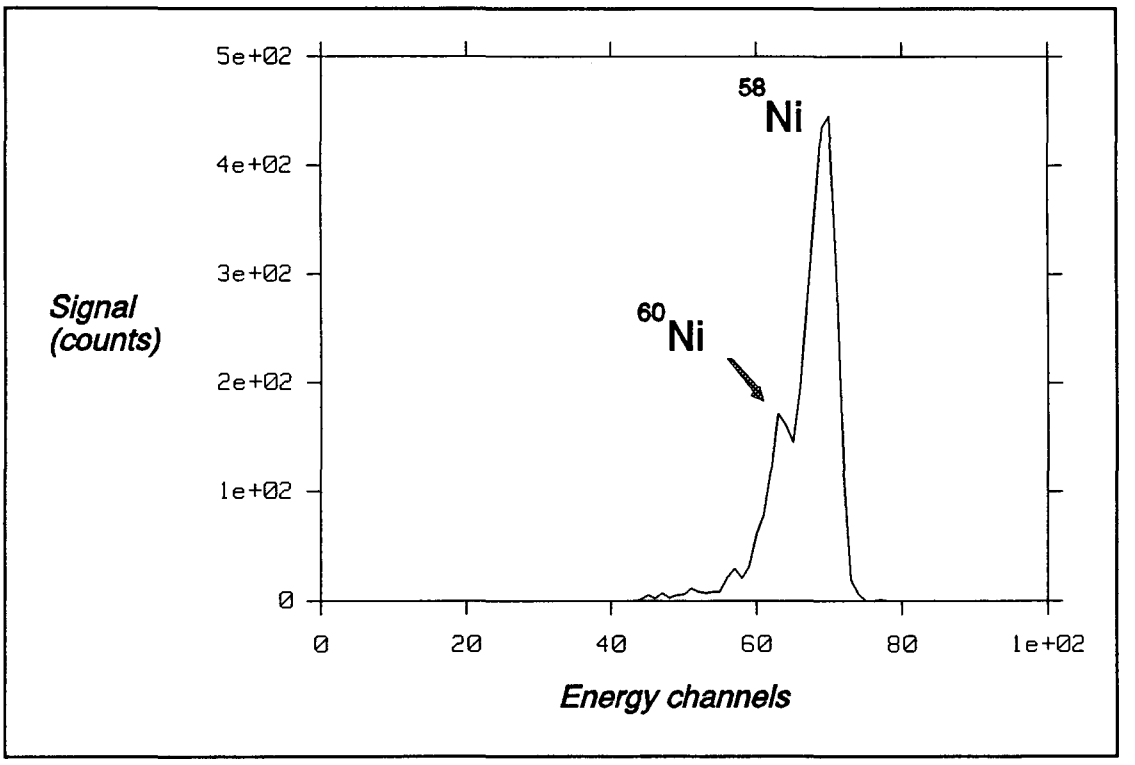

Figure 4.7: Cross-section of fig. 4.5d where we have added the azimuthal channels 68 and 69.

From the energy to position calibration we calculated the FWHM (Full Width at Half Maximum) to be 30 eV. This is better than the NODUS apparatus [BRO78] which obtained a value of 45 eV for 3 keV Ne^+ on Ni(100).

There are several effects that cause peak broadening. We will make an estimate of the contributions. The energy spread in the primary beam is only a few eV and is negligible with respect to the primary energy of 3 keV. The effect due to thermal vibrations can be estimated using equation (2.3). This gives a contribution to the FWHM of about 8 eV., for this case.

A much more important effect is the contribution due to the finite width of the accepted "beam" at the entrance of the analyzer. The effective widths of the slits were 0.4 mm for the lower one and 1 mm for the upper one. Since the distance between the last slit and the analyzer (10 mm) is small compared to the distance between the last slit and the target (100 mm), we neglect the expansion of the beam between the last slit and the analyzer. This gives an estimate of 1mm for the width of the accepted beam at the entrance of the analyzer. Hellings [HEL86] has calculated that this width expands by a factor 2 before it reaches the detector, resulting in a width of 2 mm at the detector. Since on the detector a width of 10 mm corresponds to the energy window, which is 12 % of the pass energy, the contribution to the FWHM will be 1.2 % of the pass energy. This gives a value of 24 eV.

The acceptance angle gives a spread in the scattering angle of 2.42°, which gives a contribution, due to kinematics, see equation (2.1), of about 7 eV to the FWHM. The spread in the scattering angle due to the non-parallel primary beam is estimated to be 2°, which gives a contribution of about 5 eV to the FWHM.

An important contribution is inelastic processes. As a rough estimate we assume this to be 3 % of the peak energy, which gives 24 eV.

Since these factors are independent we have to add them up quadratically, which results in an overall contribution of 36 eV. This doesn't differ to much from the obtained value of 30 eV. Although this was only a rough estimate it indicates that still improvement is possible, especially for high pass energies, by decreasing the width of the accepted beam at the entrance of the analyzer. This could

be achieved by using the focusing element at the entrance of the analyzer, which has not been tested.

Further, the EARISS apparatus is able to distinguish quite well between the Ni-isotopes ^{58}Ni(67.8%) and ^{60}Ni(26.2%) as can be seen in fig. 4.7 and fig. 4.8.

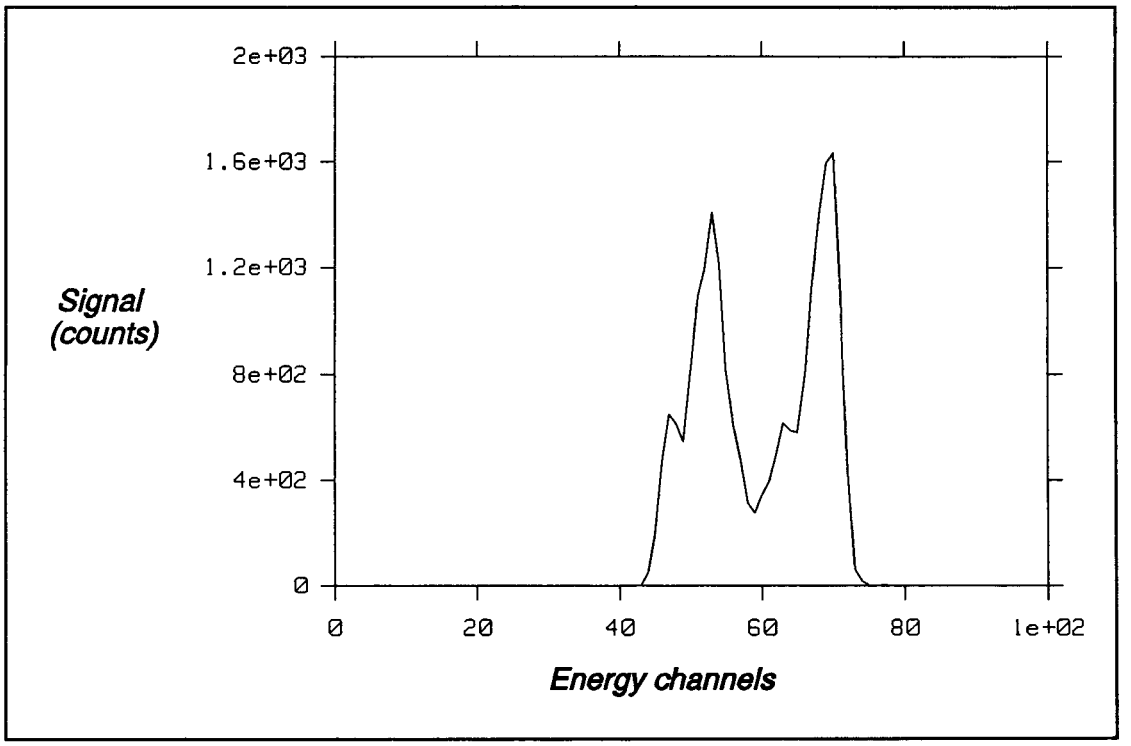

Figure 4.8: Cross-section of the sumspectra of fig. 4.5d and fig. 4.5f. The energy difference between the two peaks is 100 eV.

Fig. 4.8 is a cross-section of the sumspectra of measurements with a difference of 100 eV in the accelerating potential V3. From this difference we calculated the energy difference between the ^{58}Ni and ^{60}Ni isotope to be 35 ± 5 eV. Which agrees with the value of 39 eV obtained with the help off equation 2.1. The peak height ratio of the Ni isotopes is 2.6 which is in excellent agreement with the natural abundance of the Ni isotopes (^{58}Ni(67.8%), ^{60}Ni(26.2%), the ratio is 2.6).

Chapter 5

Static LEIS

5.1 Introduction

One of the major concerns in LEIS experiments is the damage of the surface caused by the incident ions. Especially polymers are very sensitive to ion bombardment. Hook et al. [HOO86] have shown that LEIS can provide very detailed molecular information on such surfaces when low doses are being used. The measurements performed show that the sensitivity of EARISS is such that it can be used under essentially non-destructive conditions ("Static LEIS").

5.2 Experiments

Measurements on $Au_{20}Pd_{80}$

Measurements on a $Au_{20}Pd_{80}$ alloy have been performed to illustrate the capability of the EARISS to image a relatively large part of the energy spectrum at once. Further we investigated the possibility of obtaining spectra at extremely low ion doses.

The $Au_{20}Pd_{80}$ sample was cleaned in the vacuum chamber by sputtering by the primary ion beam of 2 keV Ne^+ ions. We have to note here, that only approximately half of the azimuthal distribution could be obtained during these measurements.

Measurements on graphite

Measurements with low ion doses have been performed on a HOPG(0001)

(Highly Oriented Poly Graphite) sample, since graphite is one of the main elements that is seen when studying polymers with LEIS. Before inserting it into the vacuum system a fresh surface was obtained by pressing a piece of Scotch tape onto the surface and then removing it. Also for these measurement, we could only obtain approximately half of the azimuthal distribution.

5.3 Results and discussion

Measurements on $Au_{20}Pd_{80}$

The first measurement on $Au_{20}Pd_{80}$ as shown in fig. 5.1 was taken using 2 keV Ne^+ ions and a target current of 80 nA. The energy window was set to a width of 600 eV. This is "just" large enough to contain both the Au and Pd peaks.

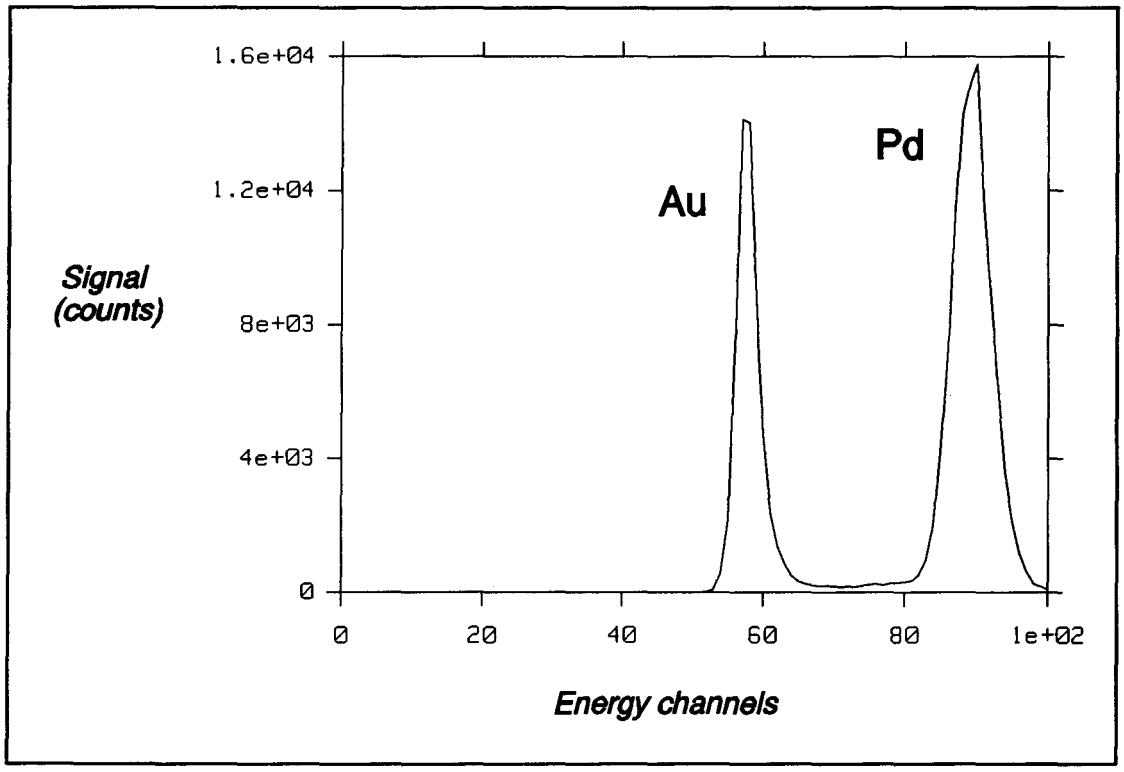

Figure 5.1: Cross-section of a spectrum of 2 keV Ne^+ → $Au_{20}Pd_{80}$, at azimuthal channel 90. The energy window was set to ≈ 600 eV.

We measured an energy difference between the peaks of 386 ± 10 eV which is

in good agreement with the theoretical value of 382 eV. The obtained FWHM for the Au and Pd peak are 62 eV and 75 eV, respectively. This is only slightly worse than the values achieved with the NODUS apparatus 46 eV for Au and 56 eV for Pd. The FWHM can be improved by narrowing the spread in the acceptance angle which was set to 3.17° (3.27 is the maximum width) in these measurements.

The major advantage of imaging several elements simultaneously is the time gained compared to most other LEIS measurements which scan a certain energy range. The energy window of the EARISS is divided in approximately 50 channels. This factor leads already to a decrease in measuring time of ~ 50 compared to a conventional LEIS apparatus which uses the same number of channels per eV.

As a comparison we show a measurement of the same sample using another LEIS apparatus, the Mini-MOBIS [HEU91], in fig. 5.2.

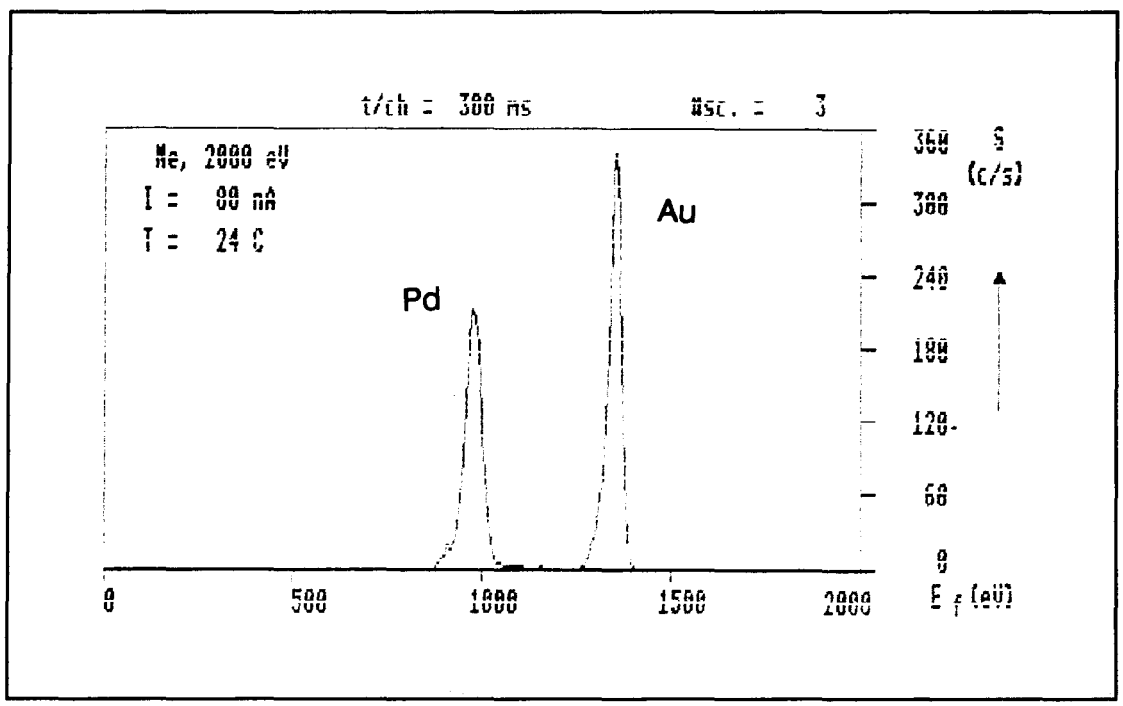

Figure 5.2: Energy spectrum of the same $Au_{20}Pd_{80}$ sample taken with the Mini-MOBIS apparatus.

The Mini-MOBIS also collects ions over the full azimuthal angle at almost the same scattering angle (144°). The difference is that it integrates over the azimuth and that energy scans are used. The energy spectrum is divided in 512 channels of 3.9 eV each. This is approximately a factor 3 smaller then the channel width of 12 eV in the EARISS measurement. If the Mini-MOBIS would also use channel widths of 12 eV we would measure a Au peak height of 3 × 340 c/s = 1020 c/s, for a target current of 80 nA, in first approximation. With EARISS we measured a Au peak height of 1.6 .10^4 C × 70 / 120 s = 9333 c/s for the same target current, where 70 is the number of azimuthal channels and 120 s the measuring time. This means that the EARISS is a factor 9 more sensitive per channel. Together with the factor 50 due to the fact that EARISS measures all the channels simultaneously, the EARISS is a factor 450 more sensitive.

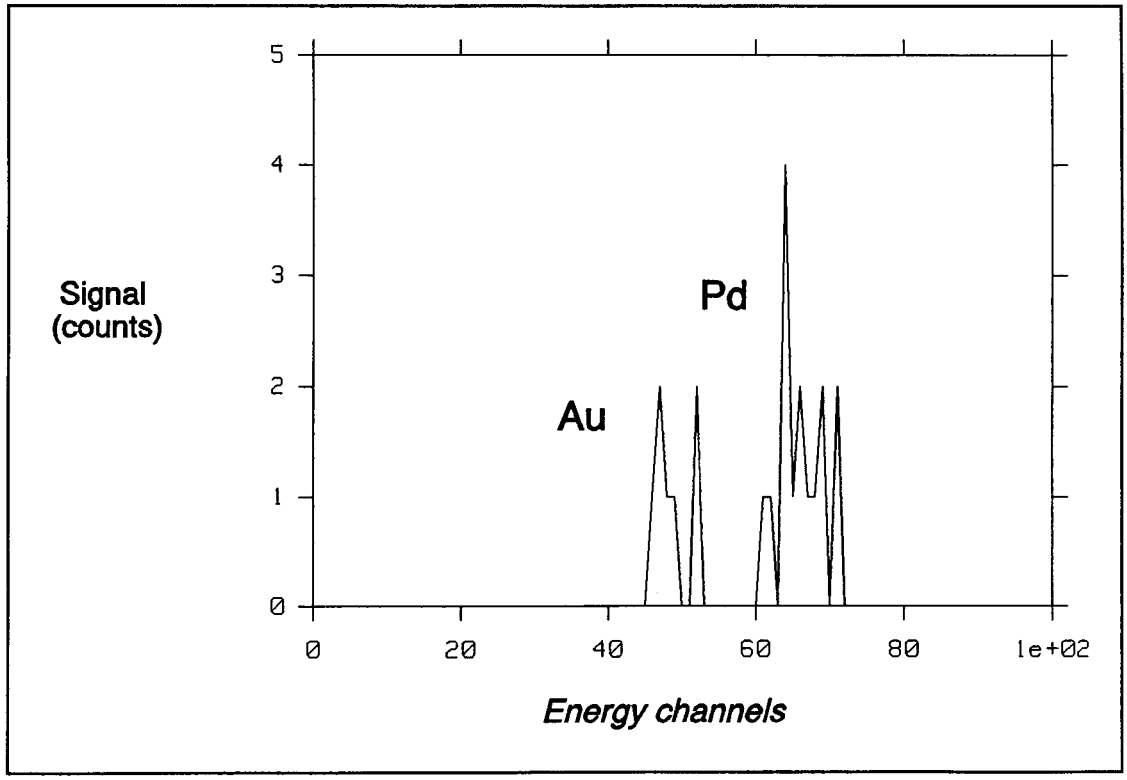

Figure 5.3a: Cross-section of a spectrum of 2 keV Ne^+ → $Au_{20}Pd_{80}$, where we have added the azimuthal channels 45 to 100. The energy window was ≈ 480 eV and the measuring time was 30 s.

Because of this higher sensitivity, it is possible to measure surface compositions with extremely low target currents as can be seen in fig. 5.3a and fig.5.3b. Here, we show spectra obtained with a target current of 3.4 pA, with measuring times of 30 s and 600 s

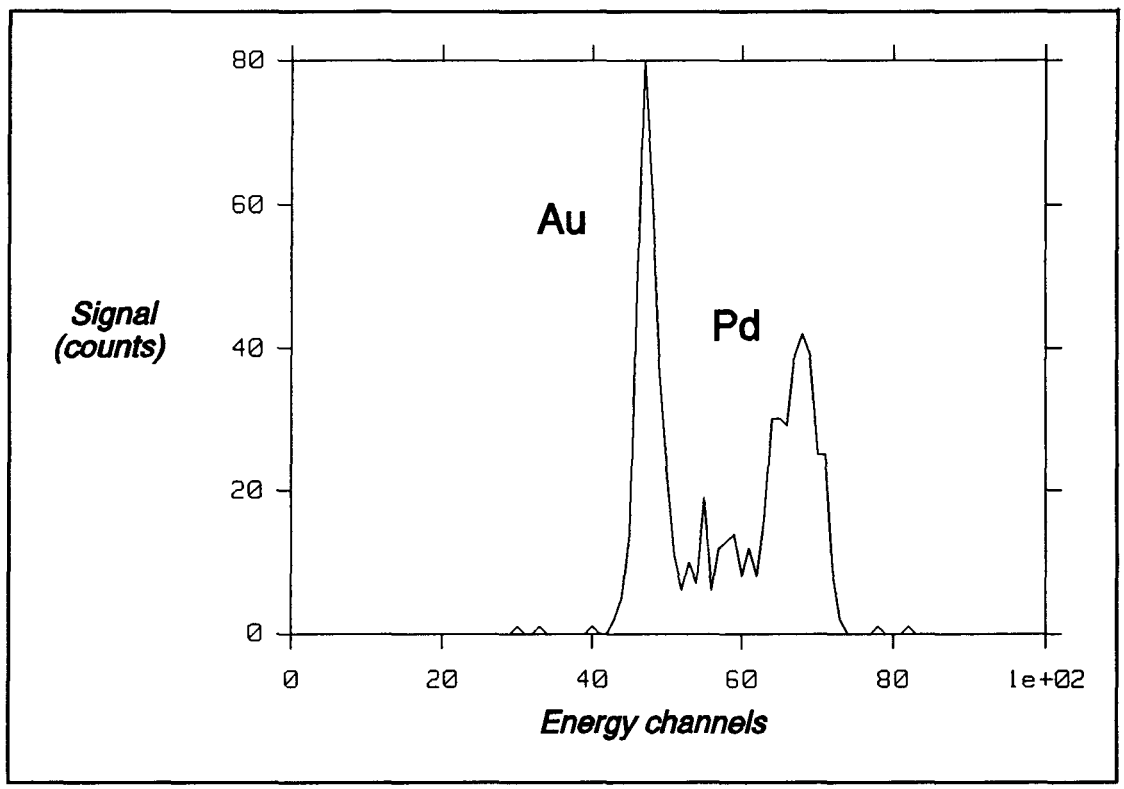

Figure 5.3b: Cross-section of a spectrum of 2 keV $Ne^+ \rightarrow Au_{20}Pd_{80}$, where we have added the azimuthal channels 45 to 100. The energy window was ≈ 480 eV and the measuring time was 600 s.

For these measurements we chose a smaller energy window of 480 eV. The Pd peak is still "entirely" visible but the Au peak lies partly outside the energy window which explains the apparently smaller FWHM compared to the measurement in fig. 5.1. The spread in the acceptance angle was increased to its maximum of value of 3.3° to obtain maximal signal. The ratio of the Pd to Au peak heights is smaller for a target current of 3.4 pA than for a target current of 80nA. (see fig. 5.1). This could be explained by the fact that Pd absorbs

contaminants which are not removed by sputtering by the incident ions, for this extremely low target current. During these measurement the base pressure was only 3. 10^{-8} mbar due to a small leak (found afterwards).

Comparing to the background, which is shown in fig. 5.4, a signal to noise ratio, based on comparison between peak heights, of better than 6 was obtained.

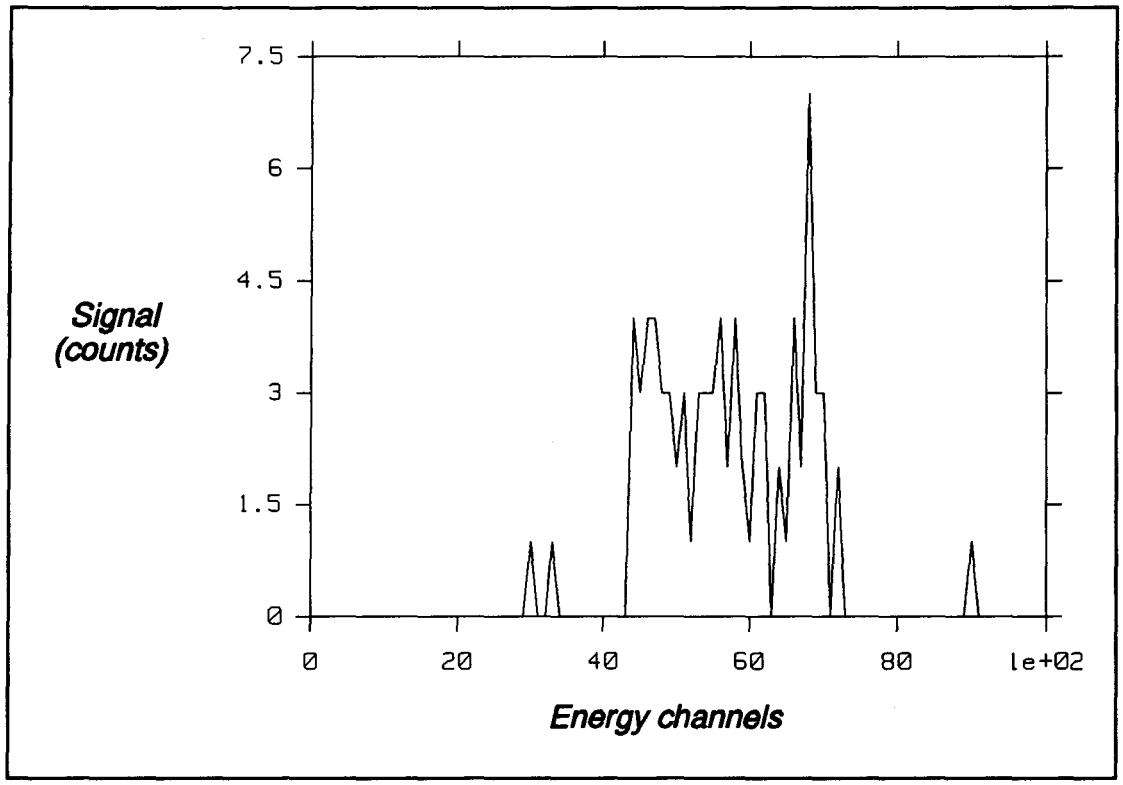

Figure 5.4: Cross-section of a spectrum taken with the primary beam off, where we have added the azimuthal channels 45 to 100. The energy window was ≈ 480 eV and the measuring time was 600 s.

Measurements on graphite

The measurements on the HOPG sample were done using 3 keV $^4He^+$ ions and a target current of 0.58 nA. It only took 30 seconds to obtain the spectrum in fig. 5.5.

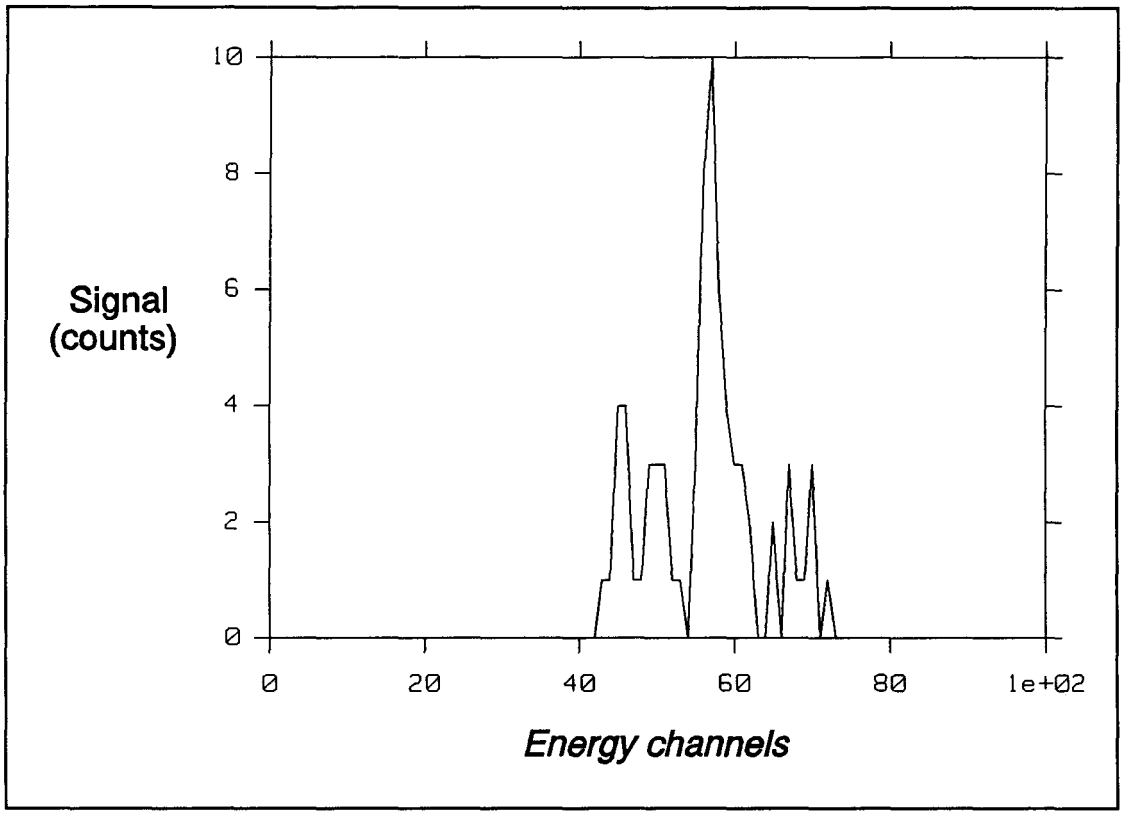

Figure 5.5: Cross-section of a spectrum of 3 keV $^4He^+$ → HOPG(0001), where we have added the azimuthal channels 50 to 100. The energy window was ≈ 480 eV and the measuring time was 30 s.

We still obtain a signal to noise ratio, better than 25.

Hook et al. [HOO86] have shown that when using 2 keV $^3He^+$ ions with a current density of 6nA/cm^2 and a measuring time smaller than 5 min no damage occurs to the surface of a polymer. Assuming a beam diameter of 1 mm we get a current density of 74 nA/cm^2 for the graphite measurements. Hook uses a current density of 6nA/cm^2 and a measuring time of 2 minutes for his polymer spectra. This gives an ion dose of 720 nC/cm^2 for one spectrum. Our graphite spectrum was taken with a dose of 2216 nC/cm^2 which is a factor 3 larger.

However, there are several easy ways to improve these measurement. Firstly, it

has to be noted that during these measurements only approximately half of the azimuthal range of the detector could be used. This means a loss of a factor 2 in signal. Secondly, by using $^3He^+$ ions the sensitivity can be increased by a factor 4. Thirdly, the diameter of the area at the target, from which scattered ions are accepted (see section 3.3) is 5.3 mm. This is larger than the beam diameter of 1 mm. So we can defocus our beam until it will covers the entire target spot and thereby decreasing the ion density. Fourthly, with our target manipulator it is possible to move the target under the ion beam during a measurement. Therefore, the ion dose can be spread out over the entire target.

Taking these considerations into account, it should be possible to perform non-destructive measurements with EARISS. Further, since the spread in our acceptance angle of 3.3° is much smaller compared to the 12° Hook uses, a better energy resolution is obtained.

Chapter 6

Detector problems

6.1 Introduction

One of the novelties of the EARISS apparatus is the high resolution charge sensitive detector. A part of the detector is the collector plate which consists of very narrow gold strips, and is, therefore, vulnerable for electrical discharges. Since the collector plate is put at a high voltage, extreme care has to be taken when changing the voltages. Even with extreme precaution electrical discharges still occur. We will describe the problem and make a hypothesis for the cause of this problem.

6.2 Detector problems

The problem with the collector plate is that every once in a while a ϕ strip blows up. This gives distorted images as can be seen in fig. 6.1a and fig. 6.1b (see next page).

The damage always occurs in the narrowest parts of the ϕ strips. This is not too surprising because there the current density will be highest. In fig. 6.1a, one sees the deformation when one of the ϕ strips is partly burned out and, therefore, interrupted. The characteristic V shape can be explained as follows: for ions with E values corresponding to the radius of the interrupted ϕ strip a too small ϕ signal is obtained this causes the spectrum to sag for that particular E value. Fig 6.1b is an example where the narrowest part of a ϕ strip did not completely burn

out.

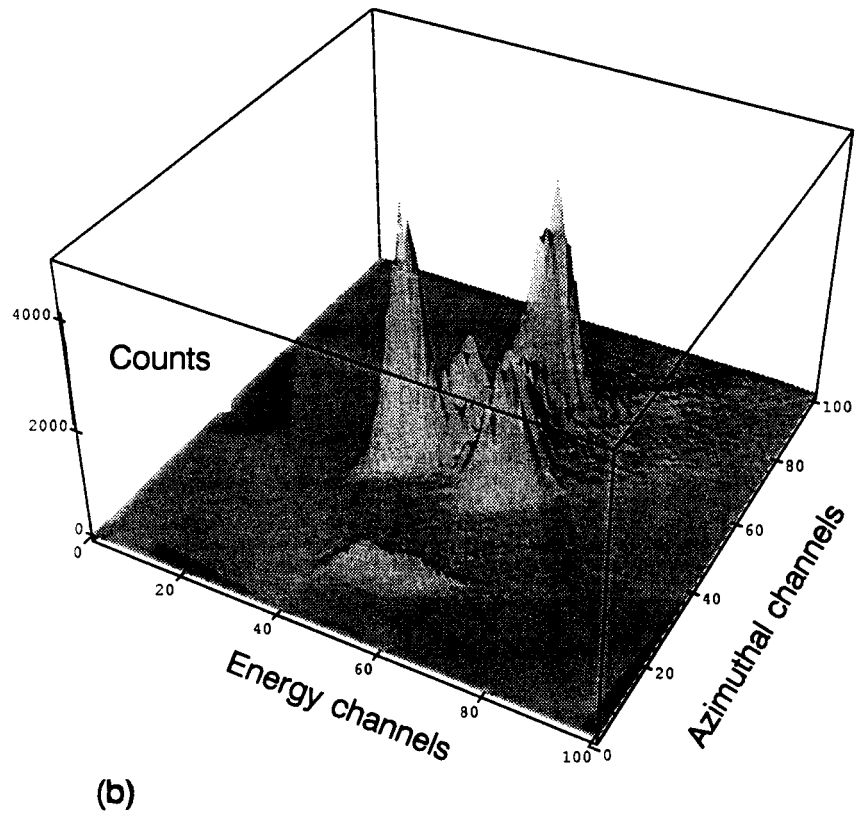

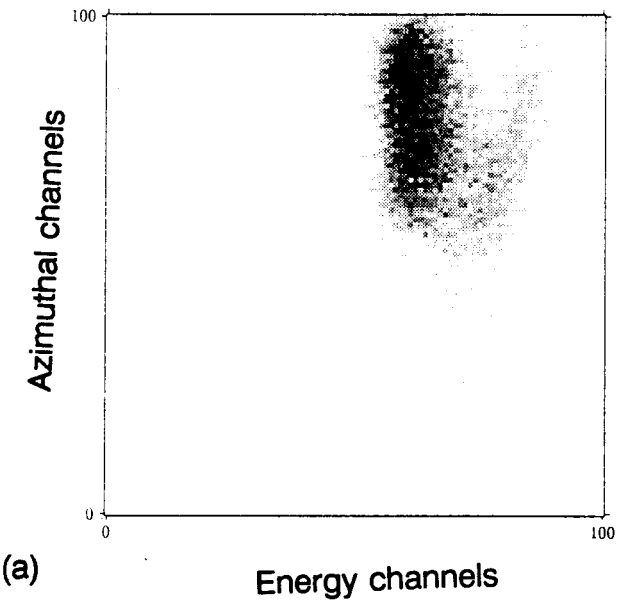

Figure 6.1: Distorted images taken with a damaged detector (explanation see text).

The diagonal in fig. 6.1b clearly indicates a correlation between the E an ϕ-signals. Later when the detector was taken out of the vacuum chamber and disassembled, it was observed that several strips were damaged. It is possible, therefore, that the shielding between the E and ϕ strips (see section 3.3) was also damaged which would explain the cross talk.

The cause of these "burn outs" are not the measurement signals themselves because the charge clouds generated by the second channelplate are way too small to cause any damage to the strips. With an amplification factor of 10^7 [ACK90] and a pulse duration of 1 ns [MEU88] we get a current of 1.6 mA during 1 ns, if we assume that all of the charge would fall on one strip (which is not the case). During a test of the collector plate a current of 50 mA was sent through a ϕ strip for several minutes without causing any noticeable heating of the strip. This could be seen from the I-V curve which was monitored during the experiment and which didn't change.

This means a discharge is most likely to cause these "burn outs". A likely hypothesis is the following. The earthing capacitor (see section 3.3) which is connected directly to the shielding strips and is attached on the back of the collector plate could deliver the power to burn out a ϕ-strip. But in order to unload this capacitor through the detector strips two discharges have two occur simultaneously. The first one is probably between one of the supply lines for the E ,ϕ and shielding strips and ground, see fig. 6.2. The second discharge, between the strips, can then not be prevented.

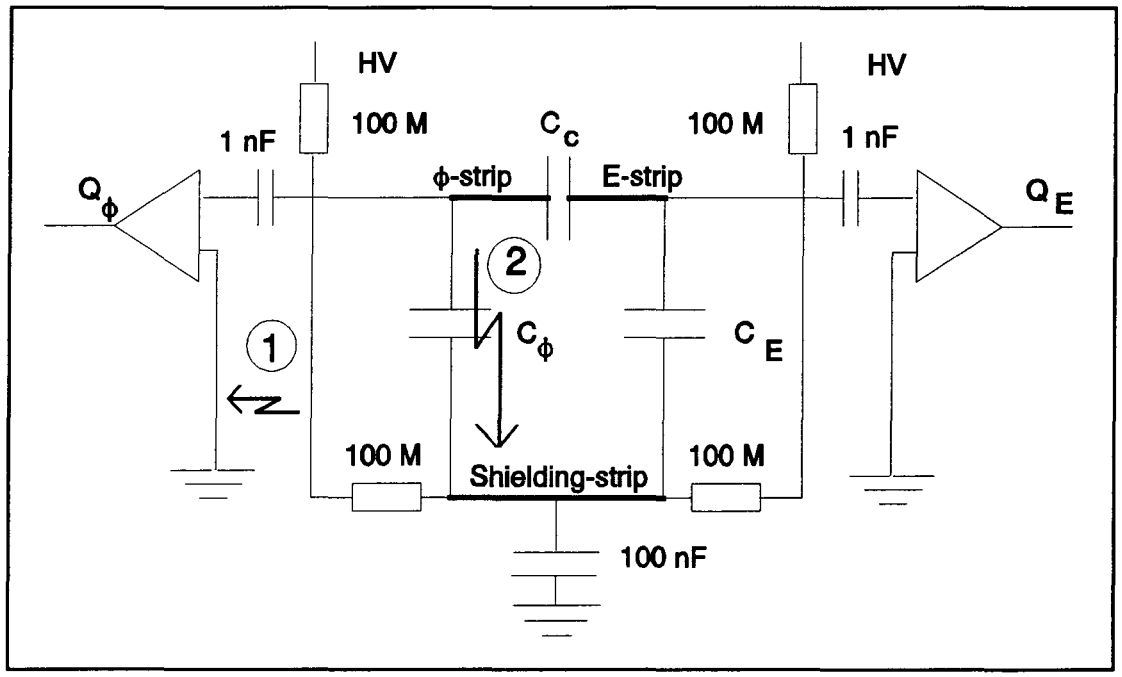

Figure 6.2: Simplified scheme of the charge collector and its connections. The discharges are indicated.

To test this hypothesis the detector will be connected to ground potential instead of to a high voltage.

This will inhibit the occurrence of the first type of discharge and, therefore, if the hypothesis is correct the detector will remain intact. This hypothesis is further supported by the fact that in a duplo apparatus of the EARISS [ACK90], which has been used to test the detector and which has a grounded detector, the detector stays undamaged.

A drawback of this solution is that the accelerating potential V3 will have a fixed value of about 3 keV. This means that the position of the energy window in the energy spectrum can only be varied by varying the pass energy. Therefore, the size and place of the energy window, within the energy spectrum, are no longer independently adjustable.

Chapter 7

Conclusions and recommendations

- The energy resolution of EARISS is good enough to clearly distinguish the Ni isotopes (^{58}Ni and ^{60} Ni) using 3 keV Ne^{+} ions.

- The energy axis of the energy window is linear except near the edges.

- It is possible to perform measurements with EARISS with extremely low ion doses. Even non-destructive measurements on polymers should be possible.

- To get a better estimate for the current density at the target, the diameter of the primary beam should be determined.

- Measurements on Ni(100) showed a peaked azimuthal distribution while, a homogeneous distribution was expected. The reason is probably the EARISS apparatus itself but is not clear yet. Further

investigation is necessary.

- Measurements on $Au_{20}Pd_{80}$ showed that it is possible, with EARISS, to measure elements, which are separated by 382 eV, simultaneously.

- Based on a hypothesis for the cause of the discharges that damage the collector plate, the collector plate was connected to ground potential instead of to a high voltage, to prevent the discharges. This change limits the flexibility of the EARISS apparatus. Therefore, if the hypothesis proves to be correct another way should be found to prevent these discharges.

References

[ACK90] P.A.J. Ackermans, PhD Thesis, Eindhoven University of Technology, 1990

[BRO76] H.H. Brongersma and T.M. Buck, Nucl. Instr. and Meth. 132 (1976) 559

[BRO78] H.H. Brongersma, N. Hazewindus, J.M. van Nieuwland, A.M.M. Otten and A.J. Smits, Rev. Sci. Instr. 49 (1978) 707

[CZA75] A.W. Czanderna, Methods of surface analysis, Elsevier scientific publishing company, 1975

[ERI75] R.L. Erickson and D.P. Smith, Phys. Rev. Lett. 132 (1975) 297

[HEL85] G.J.A. Hellings, H. Ottevanger, S.W. Boelens, C.L.C.M. Knibbeler and H.H. Brongersma, Surf. Sci 162 (1985) 913

[HEL86] G.J.A Hellings, PhD Thesis, Eindhoven University of Technology, 1986

[HAG85] H.D. Hagstrum, Phys. Rev. 96 (1954) 336

[HOO86] T.J. Hook, R.L. Schmitt, J.A. Gardella, Jr., L. Salvatti, Jr. and R.L. Chin, Anal. Chem 58 (1986) 1285

[MEU88] P.F.M. van der Meulen, Master Thesis, Eindhoven University of Technology, 1988

[TAG85] E. Taglauer, Appl. Phys. A38 (1985) 161-170

[WAL89] J.M. Walls, Methods of surface analysis, Cambridge University Press, 1989

[WIL90] W.P.M. Willems, Master Thesis, Eindhoven University of Technology, 1990

[KNI87] C.L.C.M. Knibbler et al. Rev. Sci. Instr. 58 (1987) 126

[HEU91] E. v/d Heuvel, Master Thesis, Eindhoven University of Technology, 1991